

See discussions, stats, and author profiles for this publication at: <https://www.researchgate.net/publication/351884265>

Impact of FtsZ Inhibition on the Localization of the Penicillin Binding Proteins in Methicillin-Resistant Staphylococcus aureus

Article in *Journal of Bacteriology* · May 2021

DOI: 10.1128/JB.00204-21

CITATIONS

0

READS

20

6 authors, including:



Edgar Ferrer

Reckitt Benckiser

4 PUBLICATIONS 13 CITATIONS

[SEE PROFILE](#)



Hassan Mohammed Al-Tameemi

University of Basrah

12 PUBLICATIONS 93 CITATIONS

[SEE PROFILE](#)



Jeffrey M Boyd

Rutgers, The State University of New Jersey

91 PUBLICATIONS 1,393 CITATIONS

[SEE PROFILE](#)



Daniel S Pilch

Rutgers Robert Wood Johnson Medical School, Piscataway, New Jersey

93 PUBLICATIONS 4,341 CITATIONS

[SEE PROFILE](#)

Some of the authors of this publication are also working on these related projects:



metalloprotein studies [View project](#)



Copper Intoxication in Staphylococcus aureus [View project](#)

1 Impact of FtsZ Inhibition on the Localization of the Penicillin Binding
2 Proteins in Methicillin-Resistant *Staphylococcus aureus*

3
4
5 RUNNING TITLE: Impact of FtsZ Inhibition on PBP Localization in MRSA

6
7
8 **Edgar Ferrer-González,^a Hyun Huh,^b Hassan M. Al-Tameemi,^c Jeffrey M. Boyd,^c Sang-**
9 **Hyuk Lee,^{b,d}# and Daniel S. Pilch^a#**

10

11

12 ^aDepartment of Pharmacology, Rutgers Robert Wood Johnson Medical School, Piscataway, New
13 Jersey, USA

14 ^bInstitute for Quantitative Biomedicine, Rutgers University, Piscataway, NJ, USA

15 ^cDepartment of Biochemistry and Microbiology, School of Environmental and Biological
16 Sciences, Rutgers University, New Brunswick, NJ, USA

17 ^dDepartment of Physics and Astronomy, Rutgers University, Piscataway, NJ, USA

18

19

20 #Address correspondence to Daniel S. Pilch, pilchds@rwjms.rutgers.edu or Sang-Hyuk Lee,
21 shlee@physics.rutgers.edu.

22

23 **ABSTRACT**

24 Methicillin-resistant *Staphylococcus aureus* (MRSA) is a multidrug-resistant pathogen of
25 acute clinical importance. Combination treatment with an FtsZ inhibitor potentiates the activity
26 of penicillin binding protein (PBP)-targeting β -lactam antibiotics against MRSA. To explore the
27 mechanism underlying this synergistic behavior, we examined the impact of treatment with the
28 FtsZ inhibitor TXA707 on the spatial localization of the five PBP proteins expressed in MRSA.
29 In the absence of drug treatment, PBP1, PBP2, PBP3, and PBP4 colocalize with FtsZ at the
30 septum, contributing to new cell wall formation. By contrast, PBP2a localizes to distinct foci
31 along the cell periphery. Upon treatment with TXA707, septum formation becomes disrupted
32 and FtsZ relocates away from mid-cell. PBP1 and PBP3 remain significantly colocalized with
33 FtsZ, while PBP2, PBP4, and PBP2a localize away from FtsZ to specific sites along the
34 periphery of the enlarged cells. We also examined the impact on PBP2a and PBP2 localization
35 of treatment with β -lactam antibiotic oxacillin alone and in synergistic combination with
36 TXA707. Significantly, PBP2a localizes to the septum in approximately 15% of the oxacillin-
37 treated cells, a behavior that likely contributes to the β -lactam resistance of MRSA.
38 Combination treatment with TXA707 causes both PBP2a and PBP2 to localize in malformed
39 septal-like structures. Our collective results suggest that PBP2, PBP4, and PBP2a may function
40 collaboratively in peripheral cell wall repair and maintenance in response to FtsZ inhibition by
41 TXA707. Cotreatment with oxacillin, appears to reduce the availability of PBP2a to assist in this
42 repair, thereby rendering the MRSA cells more susceptible to the β -lactam.

43

44 **IMPORTANCE**

45 MRSA is a multidrug-resistant bacterial pathogen of acute clinical importance, infecting
46 many thousands of individuals globally each year. The essential cell division protein FtsZ has
47 been identified as an appealing target for the development of new drugs to combat MRSA
48 infections. Through synergistic actions, FtsZ-targeting agents can sensitize MRSA to antibiotics
49 like the β -lactams that would otherwise be ineffective. This study provides key insights into the
50 mechanism underlying this synergistic behavior as well as MRSA resistance to β -lactam drugs.
51 The results of this work will help guide the identification and optimization of combination drug
52 regimens that can effectively treat MRSA infections and reduce the potential for future
53 resistance.

54 **INTRODUCTION**

55 Methicillin-resistant *Staphylococcus aureus* (MRSA) is a multidrug-resistant bacterial
56 pathogen that infects more than 120,000 individuals and causes nearly 20,000 deaths each year in
57 the United States (1). Growing resistance to current standard-of-care antibiotics (2-4) has
58 highlighted a critical need to develop new antibiotics that can address the MRSA threat (5-7).
59 Toward this goal, recent efforts have been focused on the development of novel small molecule
60 chemotypes that target bacterial cell division (8-12). These efforts have resulted in the
61 identification and development of lead compounds that target the essential cell division protein,
62 FtsZ (11, 13-23). Treatment of MRSA with such FtsZ inhibitors disrupts bacterial cell division
63 and induces cell death (14-18, 20, 23-26).

64 In almost all bacterial species, FtsZ plays a critical role in cell division by acting as a
65 scaffold for recruitment of other components of the cell division machinery (the divisome) (27-
66 29). FtsZ forms this scaffold by polymerizing at mid-cell and adopting a dynamic ring structure

67 termed the Z-ring (30-32). Upon formation of the Z-ring, the divisome machinery assembles,
68 with the penicillin binding proteins (PBPs) being among the key proteins that are recruited.
69 These proteins are involved in the synthesis of new cell wall at the septum (33). Methicillin-
70 sensitive *S. aureus* (MSSA) expresses a total of four PBP proteins (PBP1, PBP2, PBP3, and
71 PBP4), of which PBP1 and PBP2 have been identified as essential proteins (34). The PBP
72 proteins are targeted by β -lactam antibiotics, which disable the transpeptidase domains of the
73 proteins and thereby interfere with PBP-induced cross-linking of the bacterial cell wall (35, 36).
74 MRSA expresses an additional PBP (PBP2a) that underlies the resistance of MRSA to most β -
75 lactam antibiotics (37). The affinity of PBP2a for these β -lactam antibiotics is significantly
76 reduced compared to the other PBPs (38, 39). Co-treatment with FtsZ inhibitors can repurpose
77 β -lactam antibiotics for use against MRSA (13, 15, 25, 40, 41), with such combination
78 treatments being associated with the greatest degree of synergy when the β -lactam targets PBP2
79 with high affinity (41).

80 The mechanism underlying the potentiation of β -lactam activity against MRSA by FtsZ
81 inhibitors is unclear. Here we examine the impact of treatment with the FtsZ inhibitor TXA707
82 (18) on the localization of the five PBPs expressed in MRSA. Toward this goal, we generated a
83 series of MRSA strains expressing fluorescent fusion forms of FtsZ and either PBP1, PBP2,
84 PBP3, or PBP4. We also developed an immunofluorescence approach to monitor the
85 localization of PBP2a. Our results shed light on how FtsZ inhibitors potentiate β -lactam
86 antibiotic activity versus MRSA as well as on the mechanism by which PBP2a facilitates MRSA
87 survival in response to β -lactam antibiotic exposure.

88 RESULTS

89 **Impact of the genetic modifications on the growth and antibiotic sensitivity profile of**
90 **MRSA LAC.** After constructing our genetically modified MRSA LAC strains, we first sought
91 to explore whether our genetic alterations affected cell fitness and antibiotic sensitivity. To this
92 end, we monitored the time-dependent growth of each genetically modified strain and compared
93 the resulting growth curves to that of the wild-type LAC strain. Significantly, the growth rates of
94 the genetically modified strains were similar to that of the wild-type strain (Fig. S1), confirming
95 that our genetic alterations did not alter the fitness of the MRSA cells. We also examined the
96 sensitivity of our genetically modified strains to treatment with TXA707, vancomycin, and
97 oxacillin, as well as with the cephalosporins ceftriaxone, cefotaxime, and cephalexin. All six
98 agents were associated with similar minimal inhibitory concentrations (MICs) against wild-type
99 MRSA LAC and strains expressing FtsZ-mCherry (LAC-F_{Ch}) alone or both FtsZ-mCherry and
100 either sfGFP-PBP1 (LAC-F_{Ch}P1_{GFP}), sfGFP-PBP2 (LAC-F_{Ch}P2_{GFP}), sfGFP-PBP3 (LAC-
101 F_{Ch}P3_{GFP}) or PBP4-sfGFP (LAC-F_{Ch}P4_{GFP}) (see Table S1), indicating that these genetic
102 alterations had no impact on antibiotic sensitivity. By contrast, MRSA LAC cells expressing
103 either PBP2a-mCherry (LAC-P2A_{Ch-1}) or mCherry-PBP2a (LAC-P2A_{Ch-2}) lost their resistance to
104 oxacillin, ceftriaxone, cefotaxime, and cephalexin, with the MIC for oxacillin, ceftriaxone,
105 cefotaxime, and cephalexin against these strains being 0.125, 4, 2, and 4 µg/mL, respectively
106 (compared to corresponding MIC values of 64, 512, 128, and 128 µg/mL against the wild-type
107 strain). Significantly, the MIC values determined for oxacillin, ceftriaxone, cefotaxime, and
108 cephalexin against the MRSA LAC-P2A_{Ch-1} and LAC-P2A_{Ch-2} strains are comparable to those
109 determined for the four β-lactam antibiotics against the MSSA RN4220 strain (Table S1). Thus,
110 the PBP2a-mCherry and mCherry-PBP2a proteins were non-functional, transforming the MRSA
111 strains expressing these conjugate proteins into MSSA strains. These observations are consistent

112 with previous studies by the Pinho group indicating that appending amino acids to the *C*- or *N*-
113 terminus of PBP2a was deleterious to the localization and function of the protein (42). We
114 therefore used immunofluorescence for visualizing the localization of PBP2a (as detailed below).

115 **Impact of TXA707 treatment on MRSA cell morphology and the localization of FtsZ.** We
116 sought to determine the impact of TXA707 treatment on FtsZ localization in MRSA LAC-F_{Ch}
117 cells expressing FtsZ-mCherry. For this purpose, cells were treated with either vehicle (DMSO)
118 or 4 µg/mL TXA707 (4x MIC) for 3 hours prior to visualization by Total Internal Reflection
119 Fluorescence (TIRF) microscopy. Vehicle-treated cells ($n = 641$) maintained a normal average
120 diameter of approximately 0.84 ± 0.07 µm (Figs. 1A,H). Among the 641 vehicle-treated cells
121 analyzed, FtsZ is localized to the septum at mid-cell in 44% of them (Fig. 1I). In 16% of the
122 analyzed cells, FtsZ forms visible Z-rings (as shown in Figs. 1B,C and schematically depicted in
123 Fig. 1G). The remainder of the analyzed cells have FtsZ localized to the cell periphery (25%) or
124 in a diffuse pattern throughout the cell (14%).

125 In marked contrast to vehicle-treated cells, cells treated with TXA707 ($n = 349$) almost
126 double in size, with an average diameter of 1.50 ± 0.24 µm (Figs. 1D,H). Moreover, FtsZ is no
127 longer predominantly localized to the septum at mid-cell, with only 6% of the analyzed cells
128 exhibiting this phenotype compared to 44% of vehicle-treated cells (Fig. 1I). Instead, 43% of the
129 TXA707-treated cells have FtsZ localized in a diffuse pattern throughout the cell (compared to
130 only 14% of vehicle-treated cells with this phenotype). In addition, 39% of the 349 TXA707-
131 treated cells analyzed exhibit a phenotype in which FtsZ adopts multiple ring-shaped structures
132 inside the cell (shown in Figs. 1E,F and schematically depicted in Fig. 1G), with an average
133 diameter of 0.52 ± 0.12 µm. Thus, treatment with TXA707 increases the percentage of cells in
134 which FtsZ has formed visible ring-shaped structures by 2.4-fold (from 16% to 39%) relative to

135 vehicle treatment (Fig. 1I). Relative to vehicle, treatment with TXA707 does not induce a
136 significant change in the percentage of cells in which FtsZ is localized to the cell periphery (from
137 25% to 27%).

138 **Impact of TXA707 treatment on the localization of FtsZ relative to that of PBP1, PBP2,**
139 **PBP3, PBP4, or PBP2a in MRSA.** To understand the impact of FtsZ inhibition on the
140 localization of the five PBPs in MRSA, we generated MRSA LAC strains expressing both FtsZ-
141 mCherry as well as sfGFP fusion proteins of PBP1, PBP2, PBP3, and PBP4 (LAC-F_{Ch}P1_{GFP},
142 LAC-F_{Ch}P2_{GFP}, LAC-F_{Ch}P3_{GFP}, LAC-F_{Ch}P4_{GFP}, respectively). In addition, we also developed an
143 immunofluorescence approach to monitor the impact of FtsZ inhibition on the localization of
144 PBP2a in the LAC-F_{Ch} strain. The sections that follow describe our resulting characterizations.

145 *PBP1*: Our initial characterizations explored the impact of TXA707 treatment on MRSA
146 LAC cells expressing FtsZ-mCherry and sfGFP-PBP1 (LAC-F_{Ch}P1_{GFP}) at its native locus. In
147 vehicle-treated LAC-F_{Ch}P1_{GFP} cells ($n = 919$), PBP1 and FtsZ are localized to the septum at mid-
148 cell in 42% and 59% of the cells, respectively (see Figs. 2B-D,I,J). Most of the non-septally
149 localized PBP1 and FtsZ are localized to the cell periphery, with these phenotypes occurring in
150 49% and 29% of the analyzed cells, respectively (Fig. 2J). The remainder of the vehicle-treated
151 cells have PBP1 and FtsZ localized in a more diffuse pattern (9% of the cells in the case of PBP1
152 and 13% of cells in the case of FtsZ). Significantly, PBP1 and FtsZ colocalize in the majority
153 (70%) of the vehicle-treated LAC-F_{Ch}P1_{GFP} cells (Fig. 2J), with much of this colocalization
154 occurring at the septum and FtsZ Z-ring structures (as depicted in Figs. 2D,I).

155 Upon treatment of LAC-F_{Ch}P1_{GFP} cells ($n = 535$) with TXA707, the average cell diameter
156 increases approximately 2.1-fold from 0.84 ± 0.09 to 1.77 ± 0.27 μm (Figs. 2A,E and
157 Supplemental Fig. S2), consistent with our observations described above for LAC-F_{Ch} cells.

158 Moreover, TXA707 treatment markedly reduces the percentage of LAC-F_{Ch}P1_{GFP} cells
159 exhibiting septally-localized PBP1 from 49% to 2% (Fig. 2J). Instead, PBP1 localizes to distinct
160 foci across the cell periphery in the majority (59%) of the TXA707-treated cells analyzed (Figs.
161 2F,J). Interestingly, FtsZ appears to co-localize to those same peripheral foci (Figs. 2G-I).
162 Relative to vehicle, TXA707 treatment is also associated with a significant increase in the
163 percentage of cells exhibiting a diffuse localization phenotype for both PBP1 (from 9% to 39%)
164 and FtsZ (from 13% to 45%) (Fig. 2J). In all, PBP1 and FtsZ colocalize in 65% of the TXA707-
165 treated cells, a behavior consistent with the two proteins undergoing a similar pattern of
166 mislocalization in response to the FtsZ inhibitor.

167 PBP3: We next explored the impact of TXA707 treatment on MRSA LAC cells
168 expressing FtsZ-mCherry and sfGFP-PBP3 (LAC-F_{Ch}P3_{GFP}) at its native locus. A total of 545
169 vehicle-treated and 326 TXA707-treated LAC-F_{Ch}P3_{GFP} cells were analyzed. This analysis
170 revealed similar effects on cell diameter (Supplemental Fig. S2) as well as on PBP3 and FtsZ
171 localization phenotype (Fig. 3) to those observed in response to TXA707 treatment of LAC-
172 F_{Ch}P1_{GFP} cells. This behavior included marked TXA707-induced reductions in the septal
173 localization of both PBP3 (from 44% to 3% of cells) and FtsZ (from 58% to 3% of cells),
174 coupled with significant colocalization (in 60% of TXA707-treated cells) of both PBP3 and FtsZ
175 present in diffuse and peripheral localization phenotypes (Fig. 3H-J). These collective results
176 suggest that the FtsZ inhibitor induces a similar pattern of mislocalization between FtsZ and not
177 only PBP1, but also PBP3.

178 PBP2: We also examined the impact of TXA707 treatment on MRSA LAC cells
179 expressing FtsZ-mCherry and sfGFP-PBP2 (LAC-F_{Ch}P2_{GFP}) at its native locus, with a total of
180 1,071 vehicle-treated cells and 368 TXA707-treated cells being analyzed. The pattern of

181 observed changes in cell diameter (Figs. 4A,E and Supplemental Fig. S2) and FtsZ localization
182 (Figs. 4C,G,I,J) in response to TXA707 treatment were similar to those described above in our
183 studies of LAC-F_{Ch}P1_{GFP} and LAC-F_{Ch}P3_{GFP} cells. In vehicle-treated LAC-F_{Ch}P2_{GFP} cells, PBP2
184 localizes to the septum at mid-cell in 38% of the analyzed cells and to the cell periphery in 57%
185 of the cells (Figs. 4B,F,J). Very few (2%) of the vehicle-treated cells analyzed exhibit a
186 phenotype in which PBP2 localizes in a diffuse pattern (Fig. 4J). PBP2 colocalizes with FtsZ in
187 just over 2/3 (69%) of the vehicle-treated cells (Figs. 4D,I,J). Treatment with TXA707 induces a
188 significant decrease (from 38% to 0.2%) in cells exhibiting septally localized PBP2 and a
189 concomitant increase (from 2% to 45%) in cells exhibiting a diffuse PBP2 phenotype in which
190 multiple foci of PBP2 are distributed throughout large regions of the cell (Figs. 4F,I,J). The
191 percentage of cells in which PBP2 is localized to foci along the cell periphery does not change
192 significantly upon TXA707 treatment (Fig. 4J). While PBP2 and FtsZ colocalize in a significant
193 percentage (69%) of vehicle-treated cells, the two proteins colocalize in only 35% of TXA707-
194 treated cells (Figs. 4D,H-J). Thus, contrary to our observations described above for PBP1 and
195 PBP3, the mislocalization of PBP2 in response to TXA707 treatment appears independent of
196 FtsZ mislocalization. A similar behavior for PBP2 was previously reported by Tan *et al.* upon
197 treatment with the FtsZ inhibitor PC190723 (25).

198 PBP4: We next characterized the effects of vehicle relative to TXA707 treatment on
199 MRSA LAC cells ($n = 300$ and 326 , respectively) expressing FtsZ-mCherry and sfGFP-PBP4
200 (LAC-F_{Ch}P4_{GFP}) at its native locus. The overall impact of TXA707 treatment on LAC-F_{Ch}P4_{GFP}
201 cell diameter (Figs. 5A,E and Supplemental S2) and FtsZ localization (Figs. 5C,G,I,J) was
202 similar to that observed in LAC-F_{Ch}P1_{GFP}, LAC-F_{Ch}P2_{GFP}, and LAC-F_{Ch}P3_{GFP} cells. Like PBP1,
203 PBP2, and PBP3, PBP4 localizes to the septum in a significant percentage (55%) of vehicle-

204 treated cells, while localizing in a more diffuse pattern in a much smaller percentage (11%) of
205 cells (Figs. 5B,I,J). PBP4 localizes to the cell periphery in approximately 1/3 (33%) of the
206 vehicle-treated cells (Fig. 5J). The extent to which PBP4 colocalizes with FtsZ in vehicle-treated
207 cells is significant, with 75% of the analyzed cells exhibiting this phenotype (Figs. 5D,I,J).

208 Upon TXA707 treatment, PBP4 relocalizes away from the septum to distinct foci along
209 the cell periphery (Figs. 5F,I,J). In this connection, the percentage of cells exhibiting the septal
210 PBP4 phenotype decreases from 55% to 0.9%, while the percentage of cells exhibiting the
211 peripheral PBP4 phenotype increases from 33% to 89% (Fig. 5J). TXA707 treatment is also
212 associated with a marked reduction in the observed colocalization of PBP4 and FtsZ, with the
213 percentage of cells exhibiting this phenotype decreasing from 75% in vehicle-treated cells to
214 15% in TXA707-treated cells. Viewed as a whole, our characterizations of LAC-F_{Ch}P1_{GFP},
215 LAC-F_{Ch}P2_{GFP}, and LAC-F_{Ch}P3_{GFP}, and LAC-F_{Ch}P4_{GFP} suggest that the mislocalization of FtsZ
216 in response to treatment with the FtsZ inhibitor coincides with the mislocalization of PBP1 and
217 PBP3 but appears independent of the mislocalization of PBP2 and PBP4.

218 PBP2a: We next explored the impact of TXA707 treatment on the relative localization
219 of PBP2a and FtsZ in MRSA LAC cells expressing FtsZ-mCherry (LAC-F_{Ch}). We used an anti-
220 MRSA monoclonal antibody and immunofluorescence to visualize PBP2a in these studies, since
221 fluorescent fusion forms of PBP2a were non-functional. Prior to utilizing the antibody in our
222 immunofluorescence microscopy experiments, we verified its selectivity for PBP2a by Western
223 blot analysis using purified PBP2a as well as cell lysates of MRSA LAC, MSSA RN4220, and *E.*
224 *coli* BL21 (DE3) engineered to express *S. aureus* PBP1, PBP2, PBP3, PBP4, or PBP2a.
225 Significantly, this analysis (the results of which are shown in Supplemental Fig. S3) confirmed

226 the selectivity of the anti-MRSA antibody for PBP2a, with no observed cross-reactivity with
227 PBP1, PBP2, PBP3, or PBP4.

228 Fig. 6 shows the results of our immunofluorescence microscopy studies probing the
229 impact of TXA707 on the localization of PBP2a and FtsZ in LAC-F_{Ch} cells ($n = 536$ for vehicle
230 treatment and 315 for TXA707 treatment). In marked contrast to the behavior of PBP1, PBP2,
231 PBP3, and PBP4 in vehicle-treated cells, PBP2a does not localize to the septum at mid-cell, with
232 none of the analyzed cells exhibiting this phenotype (Figs. 6B,I,J). Instead, PBP2a localizes to
233 distinct foci across the cell periphery in the vast majority (85%) of vehicle-treated cells and in a
234 more diffuse pattern in the remaining cells. As expected, FtsZ localizes to the septum in a
235 significant percentage (48%) of vehicle-treated cells, while localizing to foci in the cell periphery
236 or in a diffuse pattern in 22% and 30% of the cells, respectively (Figs. 6C,I,J). Significantly,
237 none of the 536 vehicle-treated cells analyzed exhibit a phenotype in which FtsZ and PBP2a are
238 colocalized (Figs. 6D,I,J).

239 In response to TXA707 treatment, PBP2a localizes to an increased number of foci along
240 the periphery of the enlarged cell (Figs. 6F,I), with the overall percentage of cells exhibiting
241 peripherally localized PBP2a (81%) being similar to the 85% observed with vehicle treatment
242 (Fig. 6J). As expected, the prevalence of cells in which FtsZ is localized to the septum decreases
243 markedly (from 48% to 8%) with TXA707 treatment (Figs. 6C,G,I,J). TXA707 treatment is also
244 associated with FtsZ localization to foci in the cell periphery in 62% of the cells (Fig. 6J). As
245 observed with vehicle treatment, none of the 315 TXA707-treated cells analyzed exhibit a
246 phenotype in which FtsZ and PBP2a are colocalized (Figs. 6H,I,J). Even when both proteins are
247 localized to the cell periphery, FtsZ and PBP2a appear to form foci distinct from one another (as
248 exemplified by the cell denoted with arrow 2 in Figs. 6F-I). Like the behavior noted above for

249 PBP2 and PBP4, the relocalization of PBP2a resulting from TXA707 treatment appears to be
250 independent of the corresponding relocalization of FtsZ.

251 **Impact of treatment with the synergistic combination of TXA707 and oxacillin on cell**
252 **morphology as well as on the localization of FtsZ, PBP2a, and PBP2.** FtsZ inhibitors have
253 been shown to sensitize MRSA to β -lactam antibiotics, resulting in a synergistic antibacterial
254 effect (13, 15, 25, 40, 41). We sought to examine how treatment of MRSA LAC-F_{Ch} cells with a
255 sub-MIC concentration of TXA707 alone, oxacillin alone, or a combination of both TXA707 and
256 oxacillin impacts cell morphology as well as the localization of FtsZ and PBP2a.

257 We first compared cells treated with 2 μ g/mL (1/32x MIC) oxacillin alone ($n = 835$)
258 relative to cells treated with vehicle ($n = 535$). Oxacillin-treated cells are associated with an
259 average diameter of $1.30 \pm 0.17 \mu\text{m}$, a 1.5-fold increase relative to that ($0.86 \pm 0.13 \mu\text{m}$)
260 associated with vehicle-treated cells (Figs. 7A and 8A). In response to oxacillin treatment,
261 PBP2a localizes to the septum at mid-cell (as exemplified by the cell denoted with arrow 2 in
262 Figs. 7B,M) in 15% of the 835 cells analyzed (Fig. 8B). Significantly, this behavior markedly
263 contrasts that associated with vehicle treatment, where none of the 535 analyzed cells exhibit
264 septally localized PBP2a (Fig. 8B). Thus, treatment with oxacillin appears to induce the
265 relocalization of PBP2a to the septum in a statistically significant percentage of cells. In
266 addition, we observe oxacillin-treated cells in which PBP2a is localized to specific sites around
267 the cell periphery (as indicated by the cell denoted with arrow 1 in Figs. 7B,M), although the
268 prevalence of this PBP2a phenotype is markedly reduced (from 85% to 25%) relative to vehicle-
269 treated cells (Fig. 8B). PBP2a localizes in a more diffuse pattern in 60% of oxacillin-treated
270 cells, a rise of 45% compared to the vehicle treatment condition (Fig. 8B). FtsZ localization to
271 the septum is reduced in response to oxacillin treatment, with a concomitant increase in the

272 diffuse FtsZ phenotype (Figs. 7C,M and 8B). Significantly, in striking contrast to the absence of
273 colocalization in vehicle treated cells, FtsZ colocalizes with PBP2a in 10% of the 835 oxacillin-
274 treated cells analyzed (Fig. 8B), with this colocalization occurring almost exclusively in cells
275 where both PBP2a and FtsZ are septally localized (as indicated by the cell denoted with arrow 2
276 in Figs. 7D,M).

277 Treatment with 0.5 $\mu\text{g}/\text{mL}$ (1/2x MIC) TXA707 alone results in enlarged cells (average
278 diameter = $1.52 \pm 0.34 \mu\text{m}$) (Fig. 8A), some with oblong shapes (Figs. 7E,M), a behavior similar
279 to that observed upon treatment with 4 $\mu\text{g}/\text{mL}$ TXA707 (Figs. 6E,M). Interestingly, Pinho and
280 coworkers observed a similar oblong-shaped morphology in untreated MRSA cells expressing a
281 FtsZ variant containing the G193D mutation (43). The localization patterns for FtsZ and PBP2a
282 observed upon treatment with 0.5 $\mu\text{g}/\text{mL}$ TXA707 (Figs. 7F-H) were comparable to those
283 observed with 4 $\mu\text{g}/\text{mL}$ TXA707 treatment, with very few cells exhibiting a septal PBP2a
284 phenotype or colocalization between PBP2a and FtsZ (Fig. 8B).

285 Remarkably, co-treatment with a combination of both 2 $\mu\text{g}/\text{mL}$ oxacillin and 0.5 $\mu\text{g}/\text{mL}$
286 TXA707 yields unique morphological changes and localization patterns for both FtsZ and PBP2a
287 relative to those observed upon treatment with either agent alone. Specifically, the combination
288 treatment causes many cells to adopt oblong shapes (Figs. 7I-M), though smaller in size (average
289 diameter = $1.17 \pm 0.24 \mu\text{m}$) than those observed with TXA707 treatment alone (Fig. 8A). The
290 smaller size of the combination-treated cells relative to the cells treated with 0.5 $\mu\text{g}/\text{mL}$ TXA707
291 alone may reflect the synergistic bactericidal activity of oxacillin in combination with TXA707,
292 with this combination inducing a greater rate of kill than either agent alone (41). This enhanced
293 bactericidal activity may preclude the combination-treated cells from ever attaining the size
294 induced by treatment with TXA707 alone. In 52% of the 239 combination-treated cells analyzed

295 (Fig. 8B), PBP2a appears to localize into distinct curved structures across the cell periphery (as
296 indicated by the cells denoted with arrows 5 and 6 in Figs. 7J,M), while also localizing to the
297 septum in 24% of the combination-treated cells. FtsZ colocalizes with PBP2a in many (38%) of
298 these cells (Figs. 7L,M and 8B).

299 To gain further insight into the behavior of MRSA LAC-F_{Ch} cells in response to co-
300 treatment with the synergistic combination of oxacillin and TXA707, we sought to correlate our
301 DIC and fluorescence microscopy results shown in Fig. 7 with corresponding transmission
302 electron microscopy (TEM) studies. In these studies, the total number of cells analyzed in each
303 treatment condition were 55 for DMSO vehicle, 42 for TXA707 alone at 0.5 $\mu\text{g}/\text{mL}$ (1/2x MIC),
304 56 for oxacillin alone at 2 $\mu\text{g}/\text{mL}$ (1/32x MIC), and 53 for the combination of 2 $\mu\text{g}/\text{mL}$ oxacillin
305 and 0.5 $\mu\text{g}/\text{mL}$ TXA707. Cells treated with vehicle are round in shape and divide normally,
306 forming well-defined straight septa at mid-cell averaging approximately 40.5 nm in width (Figs.
307 9A and 10). Treatment with TXA707 alone causes the cells to enlarge significantly and disrupts
308 the ability of the cells to generate a normal septum (Fig. 9B). Approximately 48% of the
309 TXA707-treated cells analyzed appear to undergo multiple attempts at generating a septal
310 structure but are unable to complete the fully formed septum. The incomplete septal structures
311 induced by TXA707 treatment (highlighted by the white arrows Fig. 9B) are similar in width
312 (averaging 41.2 nm) to the septa formed in the presence of vehicle (Fig. 10A), with 76% of these
313 structures being straight and 24% being curved (Fig. 10B). Aberrant attempts at division in
314 TXA707-treated cells can also result in the formation of a blebs (as highlighted by the yellow
315 arrow in Fig. 9B) and a significant percentage (66%) of oblong shaped cells (Fig. 10C). 86% of
316 the cells treated with oxacillin alone were round in shape (Figs. 9C and 10C), though they appear
317 larger in size than vehicle-treated cells. The oxacillin-treated cells are still able to form complete

318 straight septa 96% of the time (Figs. 9C and 10B). However, the septa in oxacillin-treated cells
319 are approximately 2.5-times thicker than those in vehicle-treated cells (compare Figs. 9A,C),
320 averaging 100.4 nm in width (Fig. 10A). Co-treatment with the combination of TXA707 and
321 oxacillin yields a significant percentage (73%) of blebbed and oblong-shaped cells (Figs. 9D and
322 10C), with 66% of the cells exhibiting multiple thick septal-like structures (as highlighted by the
323 arrows in Fig. 9D) averaging 128.7 nm in width (Fig. 10A). 72% of these septal-like structures
324 are highly curved and irregular (Figs. 9D and 10B), similar in nature to the curved PBP2a
325 structures observed in our immunofluorescence micrographs of MRSA LAC-F_{Ch} cells treated
326 with the same combination of agents (Figs. 7J,M).

327 We also examined the impact of treatment with 2 $\mu\text{g}/\text{mL}$ oxacillin alone or in
328 combination with 0.5 $\mu\text{g}/\text{mL}$ TXA707 on the relative localization of PBP2 and FtsZ in MRSA
329 LAC-F_{Ch}P2_{GFP} cells. Both treatment conditions result in FtsZ localization patterns (Fig. S4)
330 similar to those observed in our immunofluorescence studies of MRSA LAC-F_{Ch} cells (Figs. 7
331 and 8). PBP2 localizes to the septum in 33% of the cells ($n = 406$) treated with oxacillin alone
332 (Fig. S4B,I,K). This behavior is consistent with that previously observed by Pinho and
333 Errington, who demonstrated that β -lactam treatment yields septal localization of PBP2 in
334 MRSA but not MSSA cells (44). PBP2 also localizes to foci in the cell periphery in 54% of the
335 oxacillin-treated cells analyzed, with the prevalence of both peripheral and septal PBP2 being
336 similar in oxacillin-treated relative vehicle-treated cells (Fig. S4). PBP2 colocalizes with FtsZ in
337 51% of the oxacillin-treated cells (Figs. S4D,K), compared to 69% in the vehicle treatment
338 condition. Relative to treatment with oxacillin alone, treatment of MRSA LAC-F_{Ch}P2_{GFP} cells (n
339 = 432) with a combination of both 2 $\mu\text{g}/\text{mL}$ oxacillin and 0.5 $\mu\text{g}/\text{mL}$ TXA707 results in a
340 significant reduction (from 33% to 11%) in the prevalence of PBP2 localized to the septum

341 coupled with an increase (from 54% to 72%) in the prevalence of PBP2 localized to foci in the
342 cell periphery (Fig. S4). Colocalization of PBP2 and FtsZ is also markedly reduced (from 51%
343 to 28%) with combination relative to oxacillin treatment (Figs. S4D,H,I,K).

344 **DISCUSSION**

345 FtsZ and the PBPs are key components of the divisome machinery that play important
346 roles in septum formation and cell division (32, 33, 45). FtsZ inhibitors have been shown to act
347 synergistically with PBP-targeting β -lactam antibiotics against MRSA, effectively resensitizing
348 MRSA to the β -lactams (13, 15, 25, 40, 41). To further our understanding of the basis for this
349 behavior, we examined the impact of the FtsZ inhibitor TXA707 on the relative localization of
350 FtsZ and the five PBPs in MRSA (PBP1, PBP2, PBP3, PBP4, and PBP2a). To this end, we
351 genetically engineered MRSA LAC to express a FtsZ-mCherry fusion protein and a sfGFP
352 fusion form of PBP1, PBP2, PBP3 or PBP4. We also developed an immunofluorescence
353 approach for monitoring the localization of PBP2a in MRSA LAC expressing FtsZ-mCherry.

354 In MRSA cells treated with DMSO vehicle, PBP1, PBP2, PBP3, and PBP4 are recruited
355 to FtsZ Z-rings formed at the mid-cell septum (Figs. 2-5), consistent with previous reports
356 suggesting that all four PBPs are involved in cell wall synthesis at the septum during cell
357 division (46-51). In striking contrast, PBP2a does not localize to the septum, but rather to
358 distinct foci around the cell periphery (Fig. 6). This observation suggests that under vehicle-
359 treated conditions, PBP2a is not involved in new cell wall synthesis at the septa of MRSA cells.
360 Instead, it may be functioning in cell wall maintenance and repair around the cell periphery.
361 García-Fernández *et al.* have demonstrated that PBP2a is localized in lipid rafts in MRSA cell
362 membranes (52). This observation coupled with our results suggests that the PBP2a may be

363 localized in depots around the cell periphery where it is available to act in response to conditions
364 encountered by the cell that compromise the cell wall.

365 Upon treatment with TXA707, septum formation and cell division are disrupted, with
366 FtsZ and PBP1, PBP2, PBP3 and PBP4 being mislocalized away from mid-cell (Figs. 2-5).
367 PBP1 and PBP3 relocalize to distinct foci across the cell periphery, with FtsZ co-localizing to
368 these same foci in 60%-65% of the cells analyzed (Figs. 2 and 3). This co-localization suggests
369 that PBP1 and PBP3 may function in maintaining septal integrity through direct or indirect
370 linkage with FtsZ. In contrast to the behavior of PBP1 and PBP3, PBP2 and PBP4 do not
371 significantly colocalize with FtsZ in response to FtsZ inhibition with TXA707, exhibiting a
372 colocalization phenotype in only 15%-35% of the analyzed cells. Instead, PBP2 and PBP4
373 appear to localize in foci across the cell periphery that are distinct from those in which FtsZ has
374 localized (Figs. 4 and 5). Pinho and Errington observed a similar behavior for PBP2 in
375 methicillin-sensitive *S. aureus* (MSSA) cells in which cell division had been disrupted through
376 depletion of FtsZ (53). The authors speculated that PBP2 plays a major role in the cell wall
377 remodeling and repair necessitated by the enlarged cell resulting from the block of cell division.
378 Our results suggest that both PBP2 and PBP4 are involved in such a cell wall remodeling and
379 repair process induced by FtsZ inhibition with TXA707. Interestingly, this process does not
380 appear to be coordinated by FtsZ.

381 In response to TXA707 treatment, PBP2a localizes to an increased number of foci around
382 the periphery of the enlarged cell (Fig. 6). This behavior suggests that PBP2a may play a similar
383 role to PBP2 and PBP4 in response to FtsZ inhibition, a function geared toward cell wall
384 remodeling, maintenance, and repair necessitated by a disruption of cell division. Łęski and
385 Tomasz have previously demonstrated that PBP2, PBP4, and PBP2a act cooperatively during

386 cell wall synthesis in MRSA (47). The similar behaviors we observe for PBP2, PBP4, and
387 PBP2a upon FtsZ inhibition with TXA707 are consistent with the three PBPs having cooperative
388 roles in cell wall maintenance and repair in the enlarged cells.

389 To further explore the mechanism of synergy between FtsZ inhibitors and β -lactam
390 antibiotics against MRSA, we investigated the impact of treatment with sub-MIC concentrations
391 of TXA707 alone, oxacillin alone, or a combination of both agents on the localization of FtsZ
392 and PBP2a. Upon treatment with oxacillin alone at 1/32x MIC, PBP2a relocates to the septum
393 at mid-cell (Figs. 7 and 8), suggesting that PBP2a can indeed participate in new cell wall
394 formation at the septum, but only in the presence of a β -lactam antibiotic. Although this
395 behavior was observed in only 15% of the cells analyzed, its prevalence would be more than
396 sufficient to confer MRSA with resistance to β -lactams. In addition to this localization
397 phenotype, PBP2a also localizes to multiple locations across the cell periphery, suggesting that it
398 is also involved in peripheral cell wall maintenance in response to β -lactam treatment.

399 Treatment with a synergistic combination of TXA707 and oxacillin, yields a unique
400 phenotype in which PBP2a now forms discreet curved structures across the cell periphery that
401 colocalize with FtsZ in 38% of the cells analyzed (Figs. 7J-M and 8B). This behavior differs
402 from that observed upon treatment with vehicle, TXA707 alone, or oxacillin alone. We further
403 explored this behavior using TEM. TEM micrographs of MRSA cells treated with oxacillin
404 alone revealed a substantial thickening of the septa (Figs. 9C and 10A). Recent studies by
405 Müller *et al.* have indicated that PBP2a is associated with weak transpeptidase activity, making it
406 a poor cross-linker of peptidoglycans in the bacterial cell wall (54). The thickening of the septa
407 we observe in response to oxacillin treatment may reflect the poor cross-linking activity of
408 PBP2a, which would result in a septal cell wall with reduced structural density. Additional

409 layers of peptidoglycan would have to be incorporated into the septal cell wall to compensate for
410 the reduced structural integrity, thereby resulting in a thickening of the septum. As both PBP2
411 and PBP2a are recruited to the septum upon treatment with oxacillin (Figs. 7, 8, and S4), it is
412 likely that the two proteins act collaboratively in the synthesis of new septal cell wall. This
413 hypothesis is supported by previous studies suggesting that PBP2a complements the loss of
414 PBP2 transpeptidase activity upon acylation by a β -lactam antibiotic (39, 44, 47).

415 TEM micrographs of MRSA cells treated with a synergistic combination of oxacillin and
416 TXA707 (Figs. 9 and 10) reveal a similar pattern to that observed in our immunofluorescence
417 studies (Fig. 7). In these TEM micrographs, we observe the formation of predominantly oblong-
418 shaped cells with thick, curved septal-like structures (Figs. 9D and 10) that are largely absent in
419 cells treated with either vehicle, oxacillin alone, or TXA707 alone (Fig. 10B). As noted above,
420 the thick septa observed in the presence of oxacillin may reflect a cell wall with reduced
421 structural density resulting from the poor cross-linking activity of PBP2a. Such septal structures
422 may thus be predisposed to adopt curvature in response to combination treatment with both
423 oxacillin and TXA707.

424 The unique behavior associated with the response to the combination treatment provides
425 insight into how FtsZ inhibitors can sensitize MRSA to β -lactam antibiotics. With PBP2a now
426 localizing in the curved septal-like structures that arise in response to the combination treatment,
427 it is less available to function in peripheral cell wall maintenance and repair in cooperation with
428 PBP2, which can be targeted to at least some degree by the β -lactam itself. As a result, the cell
429 would become sensitive to the β -lactam, particularly β -lactams that target PBP2 with a high
430 affinity. This hypothesis is consistent with that previously suggested by Tan *et al.* (25) as well as
431 with our previous studies demonstrating that FtsZ inhibitors synergize to the greatest extent with

432 β -lactams like oxacillin that target PBP2 with a high affinity (41). By simultaneously interfering
433 with the ability of critical PBPs (like PBP2 and PBP2a) to function in cell wall maintenance and
434 repair in response to disrupted cell division, combinations of β -lactams and FtsZ inhibitors
435 render MRSA cells more susceptible to the bactericidal effects of the β -lactams (25).

436 **ACKNOWLEDGMENTS**

437 This work was supported by NIAID grant 1R01 AI118874-05. The Boyd lab is funded by
438 NIAID grant 1R01 AI139100-01 and USDA MRF project NE-1028.

439 **MATERIALS AND METHODS**

440 **Bacterial strains and other reagents.** *S. aureus* RN4220 (MSSA) and MRSA LAC were
441 provided by the Network on Antimicrobial Resistance in *Staphylococcus aureus* (NARSA) for
442 distribution by BEI Resources, NIAID, NIH. *E. coli* NEB5 α was obtained from New England
443 Biolabs. All the MRSA LAC strains expressing fluorescent fusion forms of FtsZ and different
444 PBPs (listed in Table 1) were generated as described below. The PBP2a-specific monoclonal
445 antibody Mouse Anti-MRSA was obtained from RayBiotech (product code: 130-10096-20) and
446 the goat anti-mouse Alexa Flour 488 antibody was from ThermoFisher. Tryptic soy broth
447 (TSB), tryptic soy agar (TSA), cation-adjusted Mueller-Hinton (CAMH) media, and Luria-
448 Bertani (LB) media were obtained from Becton-Dickinson. Ampicillin sodium salt, oxacillin
449 sodium salt, cephalexin monohydrate, erythromycin, chloramphenicol, isopropyl β -D-1-
450 thiogalactopyranoside (IPTG), Tween 20, bovine serum albumin (BSA), and high-resolution
451 agarose were from Sigma. Cefotaxime and ceftriaxone sodium salts were from Toku-E.
452 Phosphate-buffered saline (PBS) was obtained from Lonza. TXA707 was synthesized as
453 previously described (18).

454 **Generation of MRSA LAC strains expressing fluorescent fusion forms of FtsZ and**
455 **different PBPs.** Fluorescent fusion proteins were cloned in MRSA LAC using the general
456 strategy outlined below. The plasmids listed in Table S2 were propagated in *E. coli* NEB5 α in
457 the presence of the appropriate antibiotic for each given plasmid. The plasmids were then
458 isolated and purified using the Monarch plasmid miniprep kit (New England Biolabs) and
459 subsequently introduced into electrocompetent *S. aureus* RN4220 cells as previously described
460 (55). Bacteriophage 80 α was used to transduce (56) the plasmids from *S. aureus* RN4220 into
461 MRSA LAC-F_{Ch}, a MRSA strain that we previously generated (57) containing an ectopic *ftsZ*-
462 *mCherry* fusion gene under control of an IPTG-inducible promoter. The MRSA LAC-F_{Ch} strains
463 expressing the fluorescent fusion form of sfGFP-PBP1, sfGFP-PBP2, sfGFP-PBP3, or PBP4-
464 sfGFP (LAC-F_{Ch}P1_{GFP}, LAC-F_{Ch}P2_{GFP}, LAC-F_{Ch}P3_{GFP}, and LAC-F_{Ch}P4_{GFP}, respectively) were
465 constructed by allelic replacement utilizing the pJB38 vector (58). In each case, DNA fragments
466 P1, P2, and P3 (see Table S3) that contain complementary overhangs were PCR amplified using
467 Q5 High-Fidelity DNA polymerase (New England Biolabs). The resulting amplified fragments
468 were then combined in equimolar quantities with the pJB38 vector, previously linearized by PCR
469 using primers pJB38-F and pJB38-R (Table S4). All four DNA fragments were then joined
470 using the NEBuilder HiFi DNA assembly kit (New England Biolabs), with each resulting
471 construct being verified by sequencing.

472 The integration of the pJB38 constructs into the MRSA LAC-F_{Ch} chromosome and
473 subsequent excision were achieved through a double recombination process, leading to an allelic
474 exchange (58, 59). Briefly, transductants containing the pJB38-derived constructs were
475 maintained at the replication-permissive temperature of 30 °C for plasmid maintenance and
476 confirmation and then frozen down. To initiate recombination, frozen stocks of the transductants

477 were streaked onto TSA plates supplemented with 30 $\mu\text{g}/\text{mL}$ chloramphenicol and 10 $\mu\text{g}/\text{mL}$
478 erythromycin and then incubated overnight at 44 $^{\circ}\text{C}$. Large colonies reflecting clones that had
479 undergone a single recombination event were restreaked onto TSA plates supplemented with 30
480 $\mu\text{g}/\text{mL}$ chloramphenicol and 10 $\mu\text{g}/\text{mL}$ erythromycin and then incubated overnight at 44 $^{\circ}\text{C}$.
481 These single recombinants were then inoculated into 5 mL of TSB and incubated at 30 $^{\circ}\text{C}$ in the
482 absence of chloramphenicol to promote a second round of recombination and subsequent
483 plasmid loss. After consecutive passages over 5 days at 30 $^{\circ}\text{C}$, the cultures were then serially
484 diluted and plated onto TSA plates supplemented with 100 ng/mL anhydrotetracycline and 10
485 $\mu\text{g}/\text{mL}$ erythromycin. To identify cells that had undergone a second recombination event and
486 subsequent loss of the plasmid, the resulting colonies were replica-patched onto TSA plates
487 supplemented with 10 $\mu\text{g}/\text{mL}$ erythromycin alone, as well as onto TSA plates supplemented with
488 both 10 $\mu\text{g}/\text{mL}$ erythromycin and 30 $\mu\text{g}/\text{mL}$ chloramphenicol. Chloramphenicol-sensitive
489 colonies were screened by PCR to verify the presence of the appropriate allele utilizing the
490 forward primer for the P1 DNA fragment and the reverse primer for the P3 DNA fragment (listed
491 in Table S3 for each denoted strain). The MRSA LAC strains expressing the fluorescent fusion
492 form of PBP2a-mCherry or mCherry-PBP2a (LAC-P2A_{Ch-1} and LAC-P2A_{Ch-2}, respectively)
493 were generated using a similar strategy to that described above, with the exception that wild-type
494 MRSA LAC was used as the recipient strain instead of MRSA LAC-F_{Ch}.

495 **Time-dependent growth assay.** An exponentially growing culture of each MRSA strain was
496 diluted in CAMH broth to a final count of 5×10^5 CFU/mL. The CFU/mL of each culture at
497 time zero was verified by plating serial dilutions in duplicate on TSA plates. The cultures were
498 then incubated at 37 $^{\circ}\text{C}$ with shaking in the presence of 100 nM IPTG to induce expression of the
499 *ftsZ-mCherry* gene when present. The CFU/mL in each culture was determined over time by

500 withdrawing samples at time points ranging from 3 to 24 hours and then plating appropriate
501 serial dilutions onto TSA plates. All TSA plates were incubated at 37°C for 24 hours and the
502 CFU/mL at each time point determined.

503 **Minimal inhibitory concentration (MIC) assay.** MIC assays were conducted in accordance
504 with Clinical and Laboratory Standards Institute (CLSI) guidelines for broth microdilution (60).
505 Briefly, log-phase MRSA cells were added to 96-well microtiter plates (at 5×10^5 CFU/mL)
506 containing 2-fold serial dilutions of TXA707, oxacillin, ceftriaxone, cefotaxime, cephalexin, or
507 vancomycin in CAMH broth, with each concentration of antibacterial agent being present in
508 duplicate. The final volume in each well was 0.1 mL, and the microtiter plates were incubated
509 aerobically for 18 hours at 37°C. Bacterial growth was monitored by measuring the optical
510 density at 600 nm (OD_{600}) using a SpectraMax M2 plate reader (Molecular Devices, Inc.), with
511 the MIC being defined as the lowest compound concentration at which growth was $\geq 90\%$
512 inhibited.

513 **Differential interference contrast (DIC) and fluorescence microscopy.** Each MRSA strain
514 was grown to log-phase in 5 mL of TSB supplemented with 10 $\mu\text{g/mL}$ erythromycin and then
515 diluted to an OD_{600} of 0.1 in 5 mL of TSB supplemented with 10 $\mu\text{g/mL}$ erythromycin. The log-
516 phase cultures were then treated with DMSO vehicle, 4 $\mu\text{g/mL}$ TXA707 (4x MIC), and 10 nM
517 IPTG for 3 hours at 37 °C. Each culture was then centrifuged at 15,000 x g for 1 minute and
518 washed twice with 1 mL of PBS. Cells were then resuspended in 200 μL of PBS. 8 μL of this
519 final cell suspension were spread on a 0.25 mm layer of 1.5% high-resolution agarose in PBS,
520 which was mounted on a petrographic 27 x 46 x 1.2 mm microscope slide (Ward's Natural
521 Science) using a 1.7 x 2.8 x 0.025 cm Gene Frame (ThermoFisher). A 24 x 40 mm cover slip

522 (Azer Scientific) was then applied to the agarose pad in preparation for microscopic
523 visualization.

524 All DIC and fluorescence microscopy experiments were conducted using a Total Internal
525 Reflection Fluorescence (TIRF) microscope that was custom-built on the basis of a commercial
526 inverted microscope (Ti-E, Nikon) (61). The microscope was equipped with a high NA
527 objective lens (CFI-apo 100X, NA 1.49, Nikon), an sCMOS camera (Zyla 4.2, Andor), and the
528 488 nm Genesis MX488-1000 STM and 561 nm Genesis MX561-1000 STM excitation lasers
529 (Coherent). For DIC imaging, a white light LED (LDB101F, Prior) was used along with Nikon's
530 DIC modules. sfGFP was imaged using 488 nm laser excitation and a green emission band pass
531 filter (ET525/50m, Chroma), while mCherry was imaged using 561 nm laser excitation and an
532 orange emission band pass filter (ET605/52m, Chroma). Multi-channel images were obtained by
533 triggered-acquisition schemes, using AOTF (AOTFnC-400.650-TN, Quanta-Tech), TTL signal
534 out of the sCMOS camera, a Data Acquisition Card (PCIe-7852R, NI), and the Nikon NIS
535 Elements software. Extra magnification was achieved using a built-in 1.5X intermediate
536 magnification changer on the microscope. MRSA samples were first inspected in the DIC
537 channel and then switched to the fluorescence channel to adjust the focus as well as the
538 excitation laser tilt angle to the optimal TIRF imaging condition. For imaging sfGFP, the 488
539 nm laser was used at power settings in the range of 2 to 15 mW, coupled with exposure times
540 ranging from 80 to 400 msec. For imaging mCherry, the 561 nm laser was used at power
541 settings in the range of 20 to 40 mW, coupled with exposure times ranging from 200 to 700
542 msec. The Perfect Focus System (Nikon) was used to actively stabilize focus drift while
543 acquiring images.

544 **Characterization of the specificity of the mouse anti-MRSA monoclonal antibody.** *E. coli*
545 BL21 (DE3) strains expressing recombinant forms of PBP1, PBP2, PBP3, or PBP4 from *S.*
546 *aureus* (SaPBP1, SaPBP2, SaPBP3, and SaPBP4, respectively) were generated as described
547 previously (41). *S. aureus* PBP2a (SaPBP2a) was cloned and expressed in *E. coli* BL21 (DE3)
548 as detailed in the Supplementary Material. For the expression of recombinant SaPBP1, SaPBP2,
549 SaPBP3, SaPBP4, and SaPBP2a, each *E. coli* strain was cultured overnight at 37 °C in LB broth
550 and then diluted 1:100 into 10 mL of LB broth. These cultures were then grown at 37 °C to an
551 OD₆₀₀ of 0.3, whereupon PBP expression was induced by the addition of 1 mM IPTG and
552 subsequent incubation for 3 hours at 37 °C. Overnight cultures of MRSA LAC and MSSA
553 RN4220 cells were diluted 1:10 into TSB and grown for 3 hours at 37 °C. The MRSA and
554 MSSA cells were then lysed by addition lysostaphin (Sigma) at a concentration of 1 mg/mL and
555 subsequent incubation for 1 hour at 37 °C.

556 All the *E. coli*, MRSA, and MSSA samples were then washed twice with 500 µL of PBS
557 and resuspended in 2 mL of PBS. The cells were sonicated for 5 minutes at 0 °C using a
558 Qsonica Q500 sonicator (equipped with a 1/8-inch probe) with an on/off cycle of 10 seconds and
559 an amplitude set at 10%. The total protein concentration in each cell lysate was then quantified
560 using a Pierce BCA Protein Assay Kit (ThermoFisher). A 12% SDS-PAGE gel (Biorad) was
561 loaded with 5 µL of 0.5 µg/mL purified recombinant SaPBP2a and 5 µL of 500 µg total
562 protein/mL from each cell lysate. Western blotting was conducted using standard procedures,
563 followed by incubation with the mouse anti-MRSA antibody (RayBiotech) at a 1:1,000 dilution.
564 Secondary antibody treatment was performed with the goat anti-mouse IgG HRP (ThermoFisher)
565 at a 1:100,000 dilution. The western blot was developed using SuperSignal West Pico PLUS
566 (ThermoFisher) solutions and visualized by chemiluminescence using an Amersham Imager 680.

567 **Immunofluorescence microscopy.** MRSA LAC-F_{Ch} cells were grown to log-phase in 5 mL of
568 TSB supplemented with 10 µg/mL erythromycin and then diluted to an OD₆₀₀ of 0.1 in 5 mL of
569 TSB supplemented with 10 µg/mL erythromycin. The log-phase cultures were then
570 supplemented with 10 nM IPTG and treated for 3 hours at 37 °C with either DMSO vehicle, 0.5
571 µg/mL TXA707 (1/2x MIC), 4 µg/mL TXA707 (4x MIC), 2 µg/mL oxacillin (1/32x MIC), or a
572 combination of 0.5 µg/mL TXA707 and 2 µg/mL oxacillin. Each culture was then centrifuged at
573 15,000 x g for 1 minute and washed twice with 1 mL of PBS. Cells were then resuspended in
574 500 µL of PBS containing 2.4% (v/v) formaldehyde, followed by incubation for 15 minutes at
575 room temperature and then 25 minutes on ice. Each culture was then centrifuged at 15,000 x g
576 for 1 minute and washed twice with 1 mL of PBS containing 0.01% Tween 20. Cells were then
577 resuspended in 500 µL of GTE buffer containing 50 mM glucose, 20 mM Tris-HCl (pH 7.6), and
578 10 mM EDTA. 100 µL of the resulting suspension was then mounted on a poly-L-Lysine-
579 coated, 18 x 18 mm cover slip (VWR). 200 µL of 30 ng/µL lysostaphin was then applied and
580 allowed to equilibrate for 1 minute. Cells were then washed three times with GTE buffer, air
581 dried, and subsequently rehydrated by applying 200 µL of PBS. After equilibration for 5
582 minutes, the cells were then blocked for 45 minutes using 300 µL of 2% (w/v) BSA. PBP2a was
583 detected via immunofluorescence using the PBP2a-specific mouse anti-MRSA monoclonal
584 antibody (RayBiotech). Serial two-fold dilutions of antibody (ranging from 1/100 to 1/1600)
585 were added to each sample and incubated overnight at 4 °C. The cells were then washed 8 times
586 with PBS and incubated in the dark for 2 hours with a goat anti-mouse Alexa Fluor 488 antibody
587 (ThermoFisher) diluted 3/1000 with PBS containing 2% (w/v) BSA. Cells were again washed 8
588 times with PBS. Aqua-Poly mounting medium (Polysciences) was then added and the cells were

589 mounted on a petrographic 27 x 46 x 1.2 mm microscope slide (Ward's Natural Science). The
590 slides were then visualized by DIC and fluorescence microscopy as described above.

591 **Transmission electron microscopy (TEM).** Log-phase MRSA LAC-F_{Ch} cells were diluted to
592 an OD₆₀₀ of 0.1 in 5 mL of TSB and then cultured at 37 °C for 3 hours in the presence of DMSO
593 vehicle, 0.5 µg/mL TXA707 (1/2x MIC), 2 µg/mL oxacillin (1/32x MIC), or a combination of
594 0.5 µg/mL TXA707 and 2 µg/mL oxacillin. The cultures were then centrifuged at 16,000 x g for
595 3 minutes at room temperature. The resulting bacterial pellets were washed with 1 mL of PBS
596 and then resuspended in 500 µL of 100 mM cacodylate buffer (pH 7.2) containing 2.5% (v/v)
597 glutaraldehyde and 4% (v/v) paraformaldehyde. The samples were then prepared for TEM
598 acquisition and the micrographs acquired as previously described (41).

599

600 **REFERENCES**

- 601 1. Kourtis AP, Hatfield K, Baggs J, Mu Y, See I, Epton E, Nadle J, Kainer MA, Dumyati G,
602 Petit S, Ray SM, Emerging Infections Program Mag, Ham D, Capers C, Ewing H, Coffin
603 N, McDonald LC, Jernigan J, Cardo D. 2019. Vital signs: Epidemiology and recent
604 trends in methicillin-resistant and in methicillin-susceptible *Staphylococcus aureus*
605 bloodstream infections - United States. MMWR Morb Mortal Wkly Rep 68:214-219.
- 606 2. Ventola CL. 2015. The antibiotic resistance crisis part 1: Causes and threats. Pharm Ther
607 40:277-83.
- 608 3. World Health Organization. 2014. Antimicrobial resistance: Global report on
609 surveillance. WHO, Geneva, Switzerland.
- 610 4. Freire-Moran L, Aronsson B, Manz C, Gyssens IC, So AD, Monnet DL, Cars O, Group
611 E-EW. 2011. Critical shortage of new antibiotics in development against multidrug-
612 resistant bacteria-Time to react is now. Drug Resist Updat 14:118-24.
- 613 5. Cars O, Hedin A, Heddini A. 2011. The global need for effective antibiotics-moving
614 towards concerted action. Drug Resist Updat 14:68-9.
- 615 6. Craft KM, Nguyen JM, Berg LJ, Townsend SD. 2019. Methicillin-resistant
616 *Staphylococcus aureus* (MRSA): Antibiotic-resistance and the biofilm phenotype.
617 MedChemComm 10:1231-1241.
- 618 7. Vestergaard M, Frees D, Ingmer H. 2019. Antibiotic resistance and the MRSA problem.
619 Microbiol Spectr 7.
- 620 8. Sass P, Brotz-Oesterhelt H. 2013. Bacterial cell division as a target for new antibiotics.
621 Curr Opin Microbiol 16:522-30.

- 622 9. Kusuma KD, Payne M, Ung AT, Bottomley AL, Harry EJ. 2019. FtsZ as an antibacterial
623 target: status and guidelines for progressing this avenue. *ACS Infect Dis* 5:1279-1294.
- 624 10. Hurley KA, Santos TM, Nepomuceno GM, Huynh V, Shaw JT, Weibel DB. 2016.
625 Targeting the bacterial division protein FtsZ. *J Med Chem* 59:6975-98.
- 626 11. Tripathy S, Sahu SK. 2019. FtsZ inhibitors as a new genera of antibacterial agents.
627 *Bioorg Chem* 91:103169.
- 628 12. Casiraghi A, Suigo L, Valoti E, Straniero V. 2020. Targeting bacterial cell division: A
629 binding site-centered approach to the most promising inhibitors of the essential protein
630 FtsZ. *Antibiotics (Basel)* 9.
- 631 13. Chan FY, Sun N, Leung YC, Wong KY. 2015. Antimicrobial activity of a quinuclidine-
632 based FtsZ inhibitor and its synergistic potential with β -lactam antibiotics. *J Antibiot*
633 68:253-8.
- 634 14. Haydon DJ, Stokes NR, Ure R, Galbraith G, Bennett JM, Brown DR, Baker PJ, Barynin
635 VV, Rice DW, Sedelnikova SE, Heal JR, Sheridan JM, Aiwale ST, Chauhan PK,
636 Srivastava A, Taneja A, Collins I, Errington J, Czaplewski LG. 2008. An inhibitor of
637 FtsZ with potent and selective anti-staphylococcal activity. *Science* 321:1673-5.
- 638 15. Kaul M, Mark L, Parhi AK, LaVoie EJ, Pilch DS. 2016. Combining the FtsZ-targeting
639 prodrug TXA709 and the cephalosporin cefdinir confers synergy and reduces the
640 frequency of resistance in methicillin-resistant *Staphylococcus aureus*. *Antimicrob*
641 *Agents Chemother* 60:4290-6.
- 642 16. Kaul M, Mark L, Zhang Y, Parhi AK, Lavoie EJ, Pilch DS. 2013. An FtsZ-targeting
643 prodrug with oral antistaphylococcal efficacy *in vivo*. *Antimicrob Agents Chemother*
644 57:5860-9.

- 645 17. Kaul M, Mark L, Zhang Y, Parhi AK, LaVoie EJ, Pilch DS. 2013. Pharmacokinetics and
646 *in vivo* antistaphylococcal efficacy of TXY541, a 1-methylpiperidine-4-carboxamide
647 prodrug of PC190723. *Biochem Pharmacol* 86:1699-707.
- 648 18. Kaul M, Mark L, Zhang Y, Parhi AK, Lyu YL, Pawlak J, Saravolatz S, Saravolatz LD,
649 Weinstein MP, LaVoie EJ, Pilch DS. 2015. TXA709, an FtsZ-targeting benzamide
650 prodrug with improved pharmacokinetics and enhanced *in vivo* efficacy against
651 methicillin-resistant *Staphylococcus aureus*. *Antimicrob Agents Chemother* 59:4845-55.
- 652 19. Margalit DN, Romberg L, Mets RB, Hebert AM, Mitchison TJ, Kirschner MW,
653 RayChaudhuri D. 2004. Targeting cell division: Small-molecule inhibitors of FtsZ
654 GTPase perturb cytokinetic ring assembly and induce bacterial lethality. *Proc Natl Acad*
655 *Sci U S A* 101:11821-6.
- 656 20. Stokes NR, Baker N, Bennett JM, Berry J, Collins I, Czaplewski LG, Logan A,
657 Macdonald R, Macleod L, Peasley H, Mitchell JP, Nayal N, Yadav A, Srivastava A,
658 Haydon DJ. 2013. An improved small-molecule inhibitor of FtsZ with superior *in vitro*
659 potency, drug-like properties, and *in vivo* efficacy. *Antimicrob Agents Chemother*
660 57:317-325.
- 661 21. Stokes NR, Baker N, Bennett JM, Chauhan PK, Collins I, Davies DT, Gavade M, Kumar
662 D, Lancett P, Macdonald R, Macleod L, Mahajan A, Mitchell JP, Nayal N, Nayal YN,
663 Pitt GR, Singh M, Yadav A, Srivastava A, Czaplewski LG, Haydon DJ. 2014. Design,
664 synthesis and structure-activity relationships of substituted oxazole-benzamide
665 antibacterial inhibitors of FtsZ. *Bioorg Med Chem Lett* 24:353-359.
- 666 22. Haydon DJ, Czaplewski LG, Stokes NR, Davies D, Collins I, Palmer JT, Mitchell JP, Pitt
667 GRW, Offermann D. 2016. Aromatic amides and uses thereof U.S. patent 9,511,073.

- 668 23. Knudson SE, Awasthi D, Kumar K, Carreau A, Goullieux L, Lagrange S, Vermet H,
669 Ojima I, Slayden RA. 2014. A trisubstituted benzimidazole cell division inhibitor with
670 efficacy against *Mycobacterium tuberculosis*. PLoS One 9:e93953.
- 671 24. Elsen NL, Lu J, Parthasarathy G, Reid JC, Sharma S, Soisson SM, Lumb KJ. 2012.
672 Mechanism of action of the cell-division inhibitor PC190723: Modulation of FtsZ
673 assembly cooperativity. J Am Chem Soc 134:12342-5.
- 674 25. Tan CM, Therien AG, Lu J, Lee SH, Caron A, Gill CJ, Lebeau-Jacob C, Benton-
675 Perdomo L, Monteiro JM, Pereira PM, Elsen NL, Wu J, Deschamps K, Petcu M, Wong
676 S, Daigneault E, Kramer S, Liang L, Maxwell E, Claveau D, Vaillancourt J, Skorey K,
677 Tam J, Wang H, Meredith TC, Sillaots S, Wang-Jarantow L, Ramtohl Y, Langlois E,
678 Landry F, Reid JC, Parthasarathy G, Sharma S, Baryshnikova A, Lumb KJ, Pinho MG,
679 Soisson SM, Roemer T. 2012. Restoring methicillin-resistant *Staphylococcus aureus*
680 susceptibility to β -lactam antibiotics. Sci Transl Med 4:126ra35.
- 681 26. Knudson SE, Awasthi D, Kumar K, Carreau A, Goullieux L, Lagrange S, Vermet H,
682 Ojima I, Slayden RA. 2015. Cell Division inhibitors with efficacy equivalent to isoniazid
683 in the acute murine *Mycobacterium tuberculosis* infection model. J Antimicrob
684 Chemother 70:3070-3.
- 685 27. Goehring NW, Beckwith J. 2005. Diverse paths to midcell: Assembly of the bacterial cell
686 division machinery. Curr Biol 15:R514-26.
- 687 28. den Blaauwen T, Hamoen LW, Levin PA. 2017. The divisome at 25: The road ahead.
688 Curr Opin Microbiol 36:85-94.
- 689 29. Margolin W. 2000. Themes and variations in prokaryotic cell division. FEMS Microbiol
690 Rev 24:531-48.

- 691 30. Ortiz C, Natale P, Cueto L, Vicente M. 2016. The keepers of the ring: Regulators of FtsZ
692 assembly. *FEMS Microbiol Rev* 40:57-67.
- 693 31. Coltharp C, Xiao J. 2017. Beyond force generation: Why is a dynamic ring of FtsZ
694 polymers essential for bacterial cytokinesis? *Bioessays* 39:1-11.
- 695 32. McQuillen R, Xiao J. 2020. Insights into the structure, function, and dynamics of the
696 bacterial cytokinetic FtsZ-ring. *Annu Rev Biophys* 49:309-341.
- 697 33. Sauvage E, Kerff F, Terrak M, Ayala JA, Charlier P. 2008. The penicillin-binding
698 proteins: Structure and role in peptidoglycan biosynthesis. *FEMS Microbiol Rev* 32:234-
699 58.
- 700 34. Reed P, Atilano ML, Alves R, Hoiczky E, Sher X, Reichmann NT, Pereira PM, Roemer
701 T, Filipe SR, Pereira-Leal JB, Ligoxygakis P, Pinho MG. 2015. *Staphylococcus aureus*
702 survives with a minimal peptidoglycan synthesis machine but sacrifices virulence and
703 antibiotic resistance. *PLoS Pathog* 11:e1004891.
- 704 35. Fernandes R, Amador P, Prudêncio C. 2013. β -Lactams: Chemical structure, mode of
705 action and mechanisms of resistance. *Rev Med Microbiol* 24:7-17.
- 706 36. Kong KF, Schneper L, Mathee K. 2010. Beta-lactam antibiotics: From antibiosis to
707 resistance and bacteriology. *APMIS* 118:1-36.
- 708 37. Peacock SJ, Paterson GK. 2015. Mechanisms of methicillin resistance in *Staphylococcus*
709 *aureus*. *Annu Rev Biochem* 84:577-601.
- 710 38. Fishovitz J, Hermoso JA, Chang M, Mobashery S. 2014. Penicillin-binding protein 2a of
711 methicillin-resistant *Staphylococcus aureus*. *IUBMB Life* 66:572-7.

- 712 39. Pinho MG, de Lencastre H, Tomasz A. 2001. An acquired and a native penicillin-binding
713 protein cooperate in building the cell wall of drug-resistant staphylococci. Proc Natl Acad
714 Sci U S A 98:10886-91.
- 715 40. Lui HK, Gao W, Cheung KC, Jin WB, Sun N, Kan JWY, Wong ILK, Chiou J, Lin D,
716 Chan EWC, Leung YC, Chan TH, Chen S, Chan KF, Wong KY. 2019. Boosting the
717 efficacy of anti-MRSA β -lactam antibiotics via an easily accessible, non-cytotoxic and
718 orally bioavailable FtsZ inhibitor. Eur J Med Chem 163:95-115.
- 719 41. Ferrer-González E, Kaul M, Parhi AK, LaVoie EJ, Pilch DS. 2017. β -Lactam antibiotics
720 with a high affinity for PBP2 act synergistically with the FtsZ-targeting agent TXA707
721 against methicillin-resistant *Staphylococcus aureus*. Antimicrob Agents Chemother
722 61:e00863-17.
- 723 42. Jorge AMR. 2012. Insights into cell wall synthesis and cell division in *Staphylococcus*
724 *aureus*. Ph.D. Thesis. Universidade NOVA de Lisboa (Portugal).
- 725 43. Pereira AR, Hsin J, Król E, Tavares AC, Flores P, Hoiczky E, Ng N, Dajkovic A, Brun
726 YV, VanNieuwenhze MS, Roemer T, Carballido-Lopez R, Scheffers DJ, Huang KC,
727 Pinho MG. 2016. FtsZ-Dependent Elongation of a Coccoid Bacterium. mBio 7.
- 728 44. Pinho MG, Errington J. 2005. Recruitment of Penicillin-Binding Protein PBP2 to the
729 Division Site of *Staphylococcus aureus* is Dependent on its Transpeptidation Substrates.
730 Mol Microbiol 55:799-807.
- 731 45. Lund VA, Wacnik K, Turner RD, Cotterell BE, Walther CG, Fenn SJ, Grein F, Wollman
732 AJ, Leake MC, Olivier N, Cadby A, Mesnage S, Jones S, Foster SJ. 2018. Molecular
733 coordination of *Staphylococcus aureus* cell division. Elife 7.

- 734 46. Pereira SF, Henriques AO, Pinho MG, de Lencastre H, Tomasz A. 2009. Evidence for a
735 dual role of PBP1 in the cell division and cell separation of *Staphylococcus aureus*. *Mol*
736 *Microbiol* 72:895-904.
- 737 47. Łęski TA, Tomasz A. 2005. Role of penicillin-binding protein 2 (PBP2) in the antibiotic
738 susceptibility and cell wall cross-linking of *Staphylococcus aureus*: evidence for the
739 cooperative functioning of PBP2, PBP4, and PBP2A. *J Bacteriol* 187:1815-24.
- 740 48. Pinho MG, de Lencastre H, Tomasz A. 2000. Cloning, characterization, and inactivation
741 of the gene *pbpC*, encoding penicillin-binding protein 3 of *Staphylococcus aureus*. *J*
742 *Bacteriol* 182:1074-9.
- 743 49. Reichmann NT, Tavares AC, Saraiva BM, Jouselin A, Reed P, Pereira AR, Monteiro
744 JM, Sobral RG, VanNieuwenhze MS, Fernandes F, Pinho MG. 2019. SEDS-bPBP pairs
745 direct lateral and septal peptidoglycan synthesis in *Staphylococcus aureus*. *Nat Microbiol*
746 4:1368-1377.
- 747 50. Monteiro JM, Fernandes PB, Vaz F, Pereira AR, Tavares AC, Ferreira MT, Pereira PM,
748 Veiga H, Kuru E, VanNieuwenhze MS, Brun YV, Filipe SR, Pinho MG. 2015. Cell
749 shape dynamics during the staphylococcal cell cycle. *Nat Commun* 6:8055.
- 750 51. Monteiro JM, Pereira AR, Reichmann NT, Saraiva BM, Fernandes PB, Veiga H, Tavares
751 AC, Santos M, Ferreira MT, Macario V, VanNieuwenhze MS, Filipe SR, Pinho MG.
752 2018. Peptidoglycan synthesis drives an FtsZ-treadmilling-independent step of
753 cytokinesis. *Nature* 554:528-532.
- 754 52. García-Fernández E, Koch G, Wagner RM, Fekete A, Stengel ST, Schneider J, Mielich-
755 Süß B, Geibel S, Markert SM, Stigloher C, Lopez D. 2017. Membrane microdomain
756 disassembly inhibits MRSA antibiotic resistance. *Cell* 171:1354-1367 e20.

- 757 53. Pinho MG, Errington J. 2003. Dispersed mode of *Staphylococcus aureus* cell wall
758 synthesis in the absence of the division machinery. *Mol Microbiol* 50:871-81.
- 759 54. Müller S, Wolf AJ, Iliev ID, Berg BL, Underhill DM, Liu GY. 2015. Poorly Cross-
760 Linked Peptidoglycan in MRSA Due to *mecA* Induction Activates the Inflammasome
761 and Exacerbates Immunopathology. *Cell Host Microbe* 18:604-12.
- 762 55. Schneewind O, Missiakas D. 2014. Genetic manipulation of *Staphylococcus aureus*. *Curr*
763 *Protoc Microbiol* 32:Unit 9C 3.
- 764 56. Novick RP. 1991. Genetic systems in staphylococci. *Methods Enzymol* 204:587-636.
- 765 57. Ferrer-González E, Fujita J, Yoshizawa T, Nelson JM, Pilch AJ, Hillman E, Ozawa M,
766 Kuroda N, Al-Tameemi HM, Boyd JM, LaVoie EJ, Matsumura H, Pilch DS. 2019.
767 Structure-guided design of a fluorescent probe for the visualization of FtsZ in clinically
768 important gram-positive and gram-negative bacterial pathogens. *Sci Rep* 9:20092.
- 769 58. Bose JL, Fey PD, Bayles KW. 2013. Genetic tools to enhance the study of gene function
770 and regulation in *Staphylococcus aureus*. *Appl Environ Microbiol* 79:2218-24.
- 771 59. Rosario-Cruz Z, Chahal HK, Mike LA, Skaar EP, Boyd JM. 2015. Bacillithiol has a role
772 in Fe-S cluster biogenesis in *Staphylococcus aureus*. *Mol Microbiol* 98:218-42.
- 773 60. Clinical and Laboratory Standards Institute. 2018. Methods for dilution antimicrobial
774 susceptibility tests for bacteria that grow aerobically, Document M07, 11th ed. CLSI,
775 Wayne, PA.
- 776 61. Lee S-H. 2018. Optimal integration of wide field illumination and holographic optical
777 tweezers for multimodal microscopy with ultimate flexibility and versatility. *Opt Express*
778 26:8049-8058.
- 779

780

TABLE 1 List of genetically modified MRSA LAC strains expressing fluorescence fusion forms of FtsZ and different PBPs

| Strain | Relevant Characteristics |
|---------------------------------------|--|
| LAC-F _{Ch} | LAC attB::[pLL39 <i>Pspac-ftsZ-mCherry lacI Tet^R</i>] pCM111- <i>lacI</i> Erm ^R |
| LAC-F _{Ch} P1 _{GFP} | LAC-F _{Ch} Δ <i>pbpA</i> :: <i>sfgfp-pbpA</i> |
| LAC-F _{Ch} P2 _{GFP} | LAC-F _{Ch} Δ <i>pbpB</i> :: <i>sfgfp-pbpB</i> |
| LAC-F _{Ch} P3 _{GFP} | LAC-F _{Ch} Δ <i>pbpC</i> :: <i>sfgfp-pbpC</i> |
| LAC-F _{Ch} P4 _{GFP} | LAC-F _{Ch} Δ <i>pbpD</i> :: <i>pbpD-sfgfp</i> |
| LAC-P2A _{Ch-1} | LAC Δ <i>mecA</i> :: <i>mecA-mCherry</i> |
| LAC-P2A _{Ch-2} | LAC Δ <i>mecA</i> :: <i>mCherry-mecA</i> |

Erm = Erythromycin, Tet = Tetracycline

781

782

783 **FIGURE LEGENDS**

784 **Figure 1:** Differential interference contrast (DIC) and fluorescence micrographs of MRSA LAC-
785 F_{Ch} cells treated for 3 hours with either DMSO vehicle (A-C) or 4 μg/mL (4x MIC) TXA707 (D-
786 F) just prior to visualization. Panels C and F depict enlargements of the regions enclosed by the
787 green and cyan boxes in panels B and E, respectively. The localization of FtsZ (red) is
788 schematically depicted in panel G, with the numbered arrows in the schematic depiction
789 reflecting the correspondingly numbered arrows in the fluorescence micrographs. The scale bars
790 for panels A-B and D-E represent 2 μm, while those for panels C and F represent 0.5 μm. The
791 bar graph in panel H shows the average diameter of the vehicle-treated cells ($n = 641$) as well as
792 the TXA707-treated cells ($n = 349$). The bar graph in panel I shows the prevalence (in %) of the
793 various FtsZ phenotypes observed in both vehicle- and TXA707-treated cells. Each percentage
794 reflects an average of 5 different fields of view, with the number of cells in each field of view
795 ranging from 56 to 171. In both panels H and I, the indicated error bars reflect the standard
796 deviation from the mean. The statistical significance of differences in cell diameter and FtsZ
797 phenotype were analyzed using a One-Way ANOVA test. **** reflects a p -value < 0.0001 ; ***
798 reflects a p -value in the range of $0.0001 < p < 0.001$; ** reflects a p -value in the range of $0.001 <$
799 $p < 0.01$; * reflects a p -value in the range of $0.01 < p < 0.1$. n.s. denotes not significant, as
800 reflected by a p -value > 0.1 .

801 **Figure 2:** DIC and fluorescence micrographs of MRSA LAC-F_{Ch}P1_{GFP} cells treated for 3 hours
802 with either DMSO vehicle (A-D) or 4 μg/mL (4x MIC) TXA707 (E-H) just prior to
803 visualization. The insets in panels B-D depict enlargements of the regions enclosed by the small
804 cyan boxes. The localization of PBP1 (green) and FtsZ (red) is schematically depicted in panel I,
805 with the numbered arrows in the scheme reflecting the correspondingly numbered arrows in the

806 fluorescence micrographs. The scale bars for panels A-H represent 2 μm , while those for the
807 insets in panels B-D represent 0.5 μm . The bar graph in panel J shows the prevalence (in %) of
808 the various FtsZ and PBP1 phenotypes observed in both vehicle-treated cells ($n = 919$) and
809 TXA707-treated cells ($n = 535$). Each percentage reflects an average of 5 different fields of
810 view, with the number of cells in each field of view ranging from 98 to 256. The indicated error
811 bars reflect the standard deviation from the mean. The statistical significance of differences in
812 the FtsZ and PBP1 phenotypes were analyzed as described in the legend to Fig. 1. n.s. denotes
813 not significant.

814 **Figure 3:** DIC and fluorescence micrographs of MRSA LAC-F_{Ch}P3_{GFP} cells treated as described
815 in the legend to Fig. 2. The localization of PBP3 (green) and FtsZ (red) is schematically
816 depicted in panel I, with the numbered arrows in the scheme reflecting the correspondingly
817 numbered arrows in the fluorescence micrographs. The scale bars for panels A-H represent 2 μm .
818 The bar graph in panel J shows the prevalence (in %) of the various FtsZ and PBP3 phenotypes
819 observed in both vehicle-treated cells ($n = 545$) and TXA707-treated cells ($n = 326$). Each
820 percentage reflects an average of 5 different fields of view, with the number of cells in each field
821 of view ranging from 48 to 136. The indicated error bars reflect the standard deviation from the
822 mean. The statistical significance of differences in the FtsZ and PBP3 phenotypes were analyzed
823 as described in the legend to Fig. 1.

824 **Figure 4:** DIC and fluorescence micrographs of MRSA LAC-F_{Ch}P2_{GFP} cells treated as described
825 in the legend to Fig. 2. The localization of PBP2 (green) and FtsZ (red) is schematically
826 depicted in panel I, with the numbered arrows in the scheme reflecting the correspondingly
827 numbered arrows in the fluorescence micrographs. The scale bars for panels A-H represent 2 μm .
828 The bar graph in panel J shows the prevalence (in %) of the various FtsZ and PBP2 phenotypes

829 observed in both vehicle-treated cells ($n = 1,071$) and TXA707-treated cells ($n = 368$). Each
830 percentage reflects an average of 5 different fields of view, with the number of cells in each field
831 of view ranging from 44 to 247. The indicated error bars reflect the standard deviation from the
832 mean. The statistical significance of differences in the FtsZ and PBP2 phenotypes were analyzed
833 as described in the legend to Fig. 1. n.s. denotes not significant.

834 **Figure 5:** DIC and fluorescence micrographs of MRSA LAC-F_{Ch}P4_{GFP} cells treated as described
835 in the legend to Fig. 2. The localization of PBP4 (green) and FtsZ (red) is schematically
836 depicted in panel I, with the numbered arrows in the scheme reflecting the correspondingly
837 numbered arrows in the fluorescence micrographs. The scale bars for panels A-H represent 2 μm .
838 The bar graph in panel J shows the prevalence (in %) of the various FtsZ and PBP4 phenotypes
839 observed in both vehicle-treated cells ($n = 300$) and TXA707-treated cells ($n = 326$). Each
840 percentage reflects an average of 3 to 5 different fields of view, with the number of cells in each
841 field of view ranging from 56 to 162. The indicated error bars reflect the standard deviation
842 from the mean. The statistical significance of differences in the FtsZ and PBP4 phenotypes were
843 analyzed as described in the legend to Fig. 1. n.s. denotes not significant.

844 **Figure 6:** DIC and fluorescence micrographs of MRSA LAC-F_{Ch} cells treated for 3 hours with
845 either DMSO vehicle (A-D) or 4 $\mu\text{g}/\text{mL}$ (4x MIC) TXA707 (panels E-H), followed by
846 immunostaining using a PBP2a-specific monoclonal mouse antibody and a goat anti-mouse
847 Alexa Fluor® 488 secondary antibody prior visualization. The localization of PBP2a (green)
848 and FtsZ (red) is schematically depicted in panel I, with the numbered arrows in the scheme
849 reflecting the correspondingly numbered arrows in the fluorescence micrographs. The scale bars
850 for panels A-H represent 2 μm . The bar graph in panel J shows the prevalence (in %) of the
851 various FtsZ and PBP2a phenotypes observed in both vehicle-treated cells ($n = 536$) and

852 TXA707-treated cells ($n = 315$). Each percentage reflects an average of 5 different fields of
853 view, with the number of cells in each field of view ranging from 29 to 116. The indicated error
854 bars reflect the standard deviation from the mean. The statistical significance of differences in
855 the FtsZ and PBP2a phenotypes were analyzed as described in the legend to Fig. 1. n.s. denotes
856 not significant, while n.o. denotes none observed.

857 **Figure 7:** DIC and fluorescence micrographs of MRSA LAC-F_{Ch} cells treated for 3 hours with
858 either 2 $\mu\text{g/mL}$ (1/32x MIC) oxacillin (A-D), 0.5 $\mu\text{g/mL}$ (1/2x MIC) TXA707 (panels E-H), or a
859 combination of 2 $\mu\text{g/mL}$ oxacillin and 0.5 $\mu\text{g/mL}$ TXA707 (panels I-L), followed by
860 immunostaining of PBP2a as described in the legend to figure 6. The localization of PBP2a
861 (green) and FtsZ (red) is schematically depicted in panel M, with the numbered arrows in the
862 scheme reflecting the correspondingly numbered arrows in the fluorescence micrographs. The
863 scale bars for panels A-L represent 2 μm .

864 **Figure 8:** Quantification of the cell diameter, FtsZ phenotype, and PBP2a phenotype results of
865 the microscopy experiments depicted in Fig. 7. The bar graph in panel A shows the average
866 diameter of the vehicle-treated cells ($n = 535$), oxacillin-treated cells ($n = 835$), TXA707-treated
867 cells ($n = 270$), and the cells treated with a combination of both oxacillin and TXA707 ($n = 239$).
868 The bar graph in panel B shows the prevalence (in %) of the various FtsZ and PBP2a phenotypes
869 observed in the different treatment groups. Each percentage reflects an average of 5 to 6
870 different fields of view, with the number of cells in each field of view ranging from 28 to 325. In
871 both panels A and B, the indicated error bars reflect the standard deviation from the mean. The
872 statistical significance of differences in cell diameter, FtsZ phenotype, and PBP2a phenotype
873 were analyzed as described in the legend to Fig. 1. n.s. denotes not significant, while n.o.
874 denotes none observed.

875 **Figure 9:** Transmission electron micrographs of MRSA LAC-F_{Cb} cells treated for 3 hours with
876 either vehicle (A), 0.5 µg/mL TXA707 alone (B), 2 µg/mL oxacillin alone (C), or 0.5 µg/mL
877 TXA707 in combination with 2 µg/mL oxacillin (D). The scale bars for panels A-D represent
878 0.2 µm. The white arrows in panels A and C highlight septa in dividing cells, while the white
879 arrows in panels B and D highlight incomplete or aberrant septal structures. The yellow arrow in
880 panel B highlights a bleb resulting from an aberrant attempt at division.

881 **Figure 10:** Quantification of the septal structure width (A), septal structure phenotype (B), and
882 cell shape (C) for the results of the TEM experiments depicted in Fig. 9. The bar graph in panel
883 A shows the average septal structure width with vehicle treatment ($n = 55$), oxacillin treatment (n
884 $= 72$), TXA707 treatment ($n = 78$), or treatment with a combination of both oxacillin and
885 TXA707 ($n = 106$). The bar graph in panel B shows the prevalence (in %) of the septal structure
886 phenotype (straight vs. curved) observed in the different treatment groups. The bar graph in
887 panel C shows the prevalence (in %) of the cell shape (round vs. oblong) observed in the
888 different treatment groups ($n = 55$ for vehicle, $n = 56$ for oxacillin alone, $n = 42$ for TXA707
889 alone, and $n = 53$ for the combination). In both panels B and C, each percentage reflects an
890 average of 14-18 different fields of view, with the indicated error bars reflecting the standard
891 deviation from the mean. The statistical significance of differences in septal structure width,
892 septal structure phenotype, and cell shape were analyzed as described in the legend to Fig. 1. n.s.
893 denotes not significant, while n.o. denotes none observed.

Figure 1

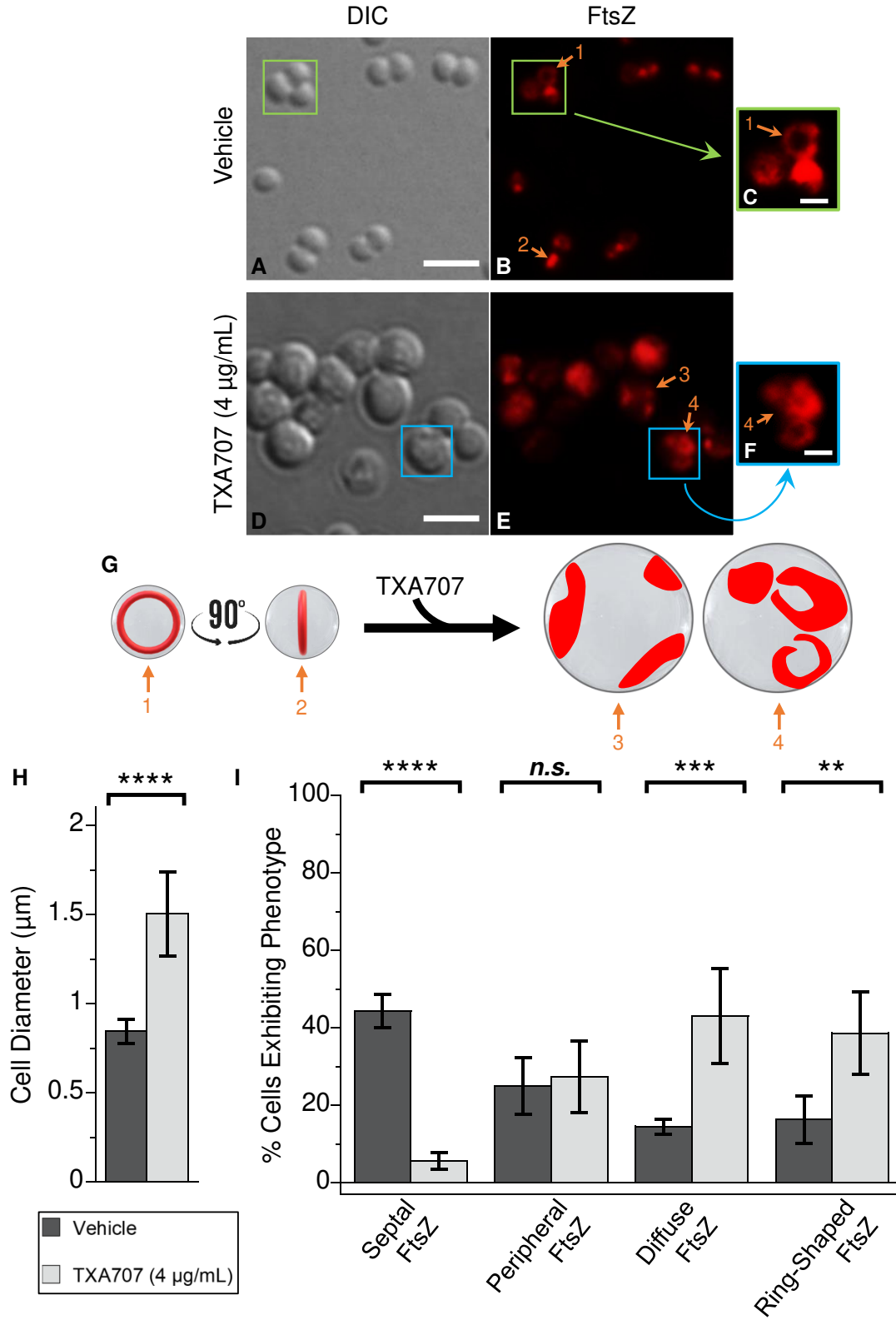


Figure 2

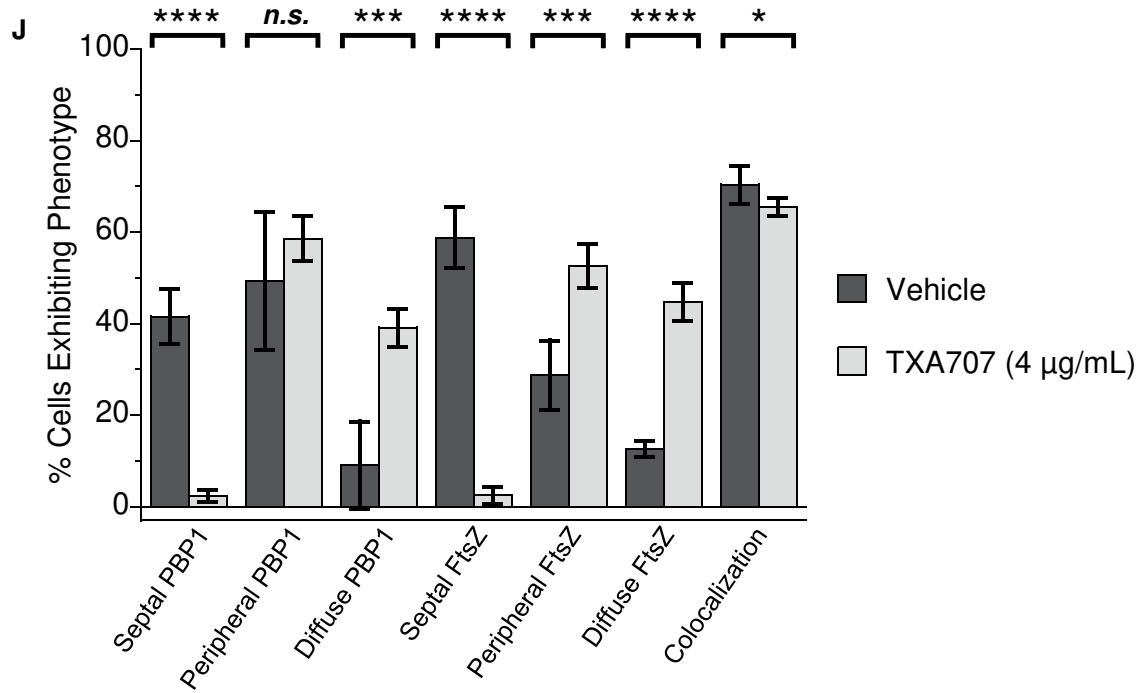
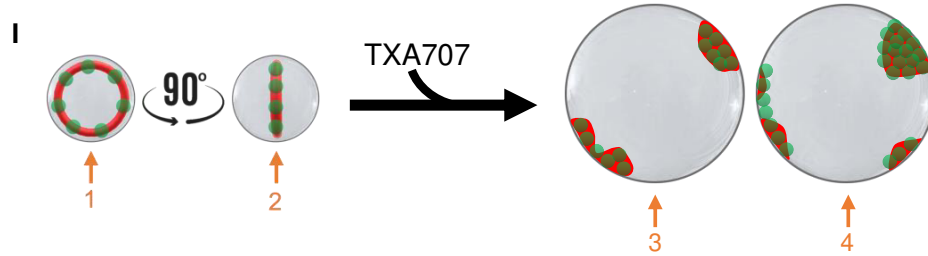
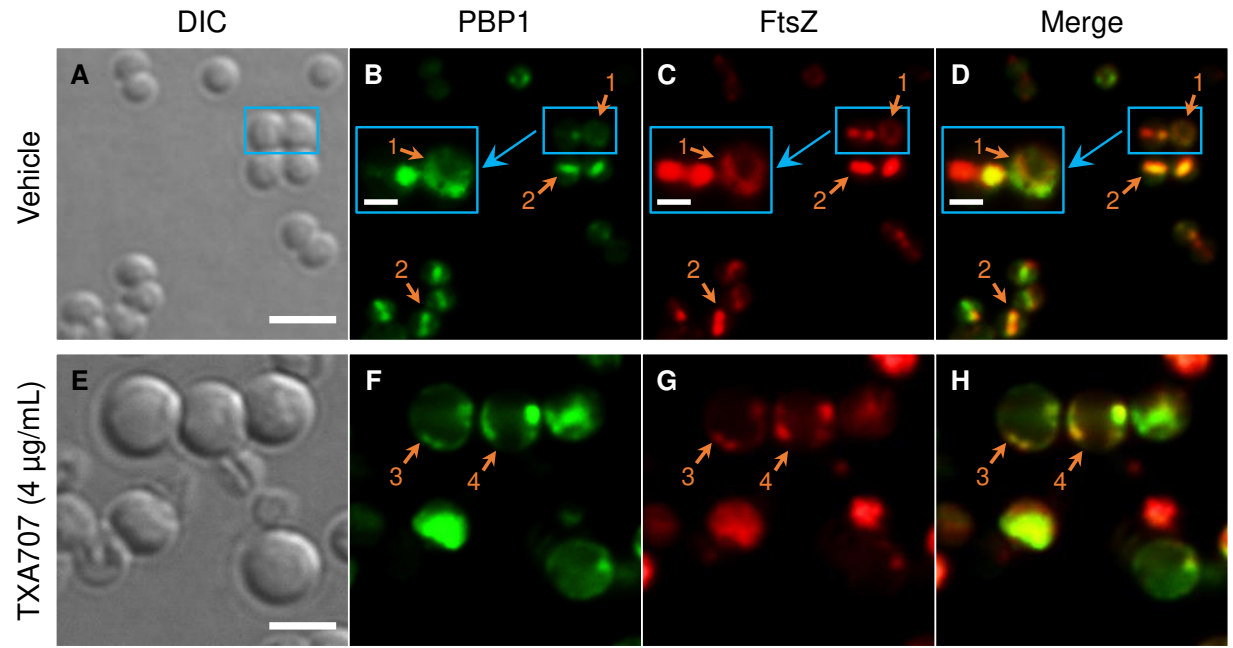


Figure 3

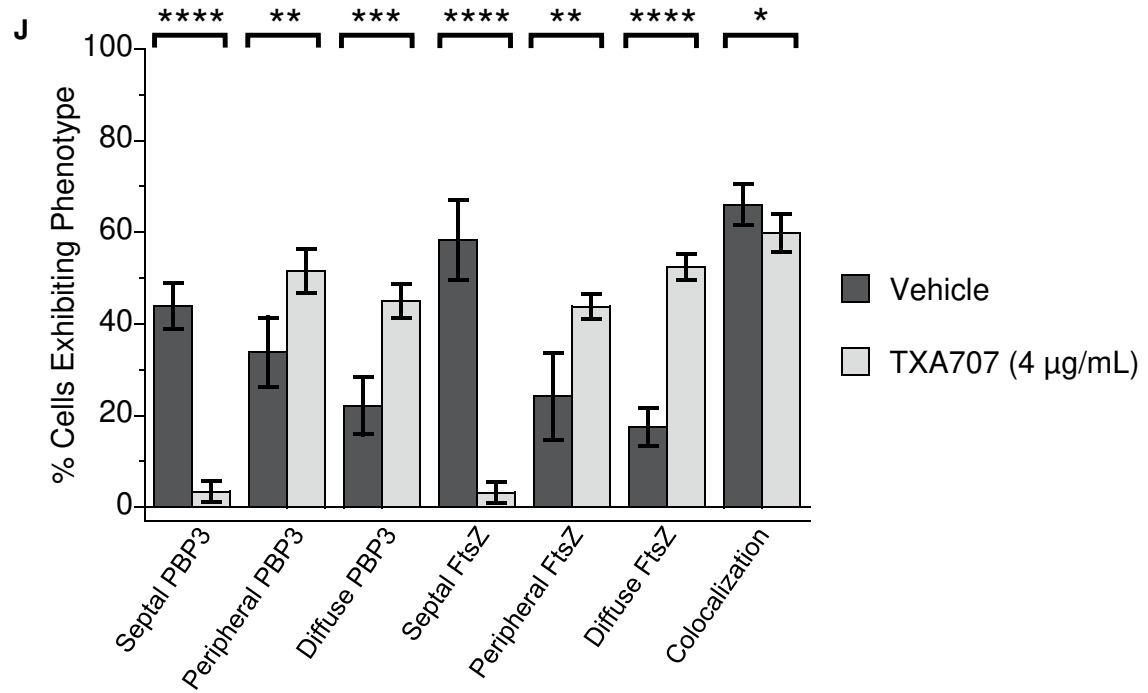
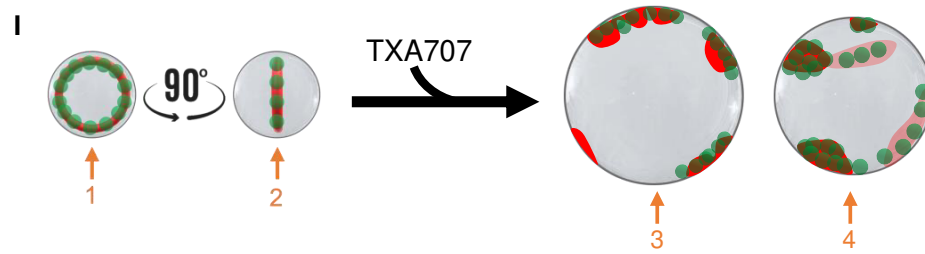
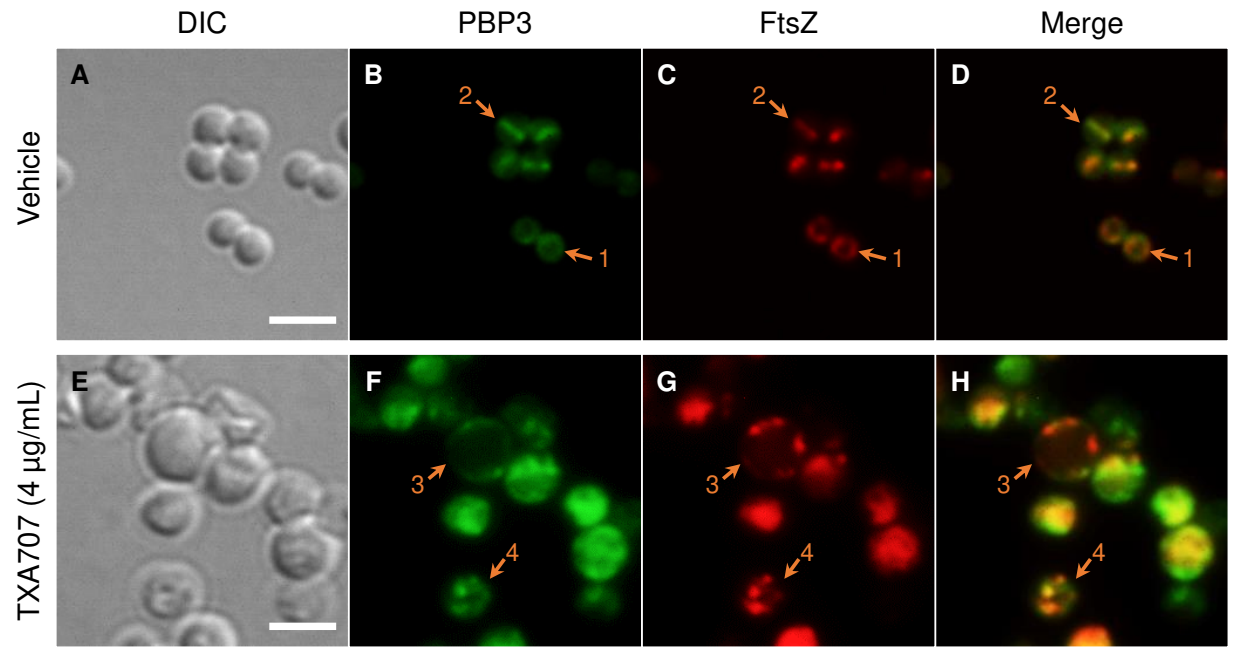


Figure 4

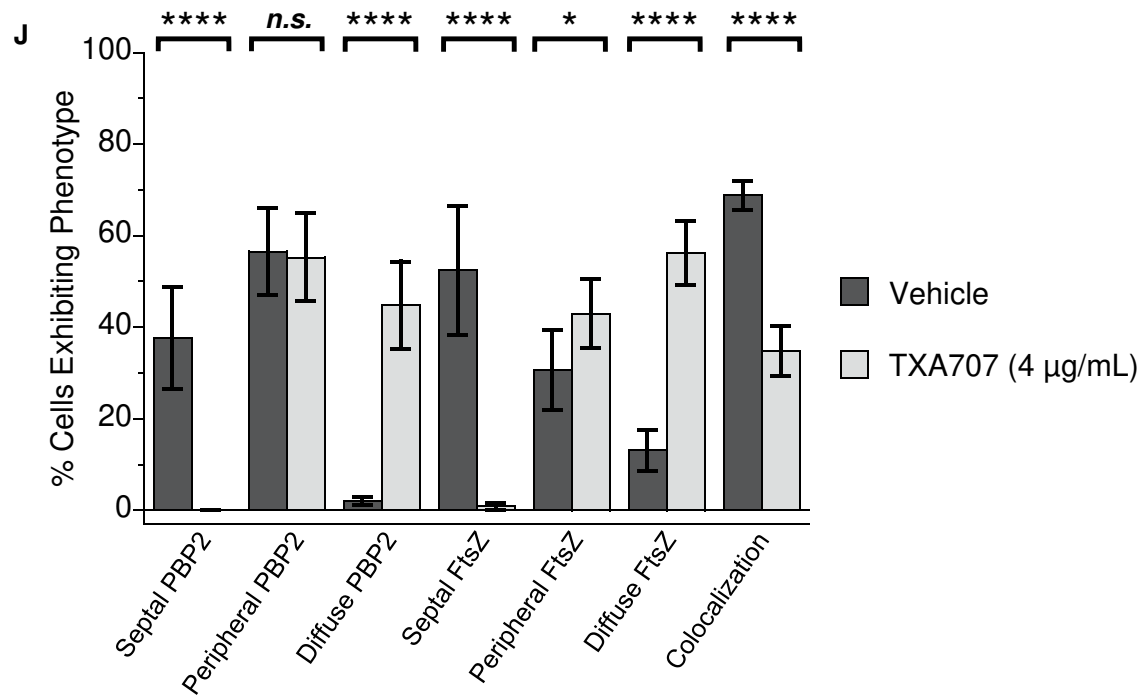
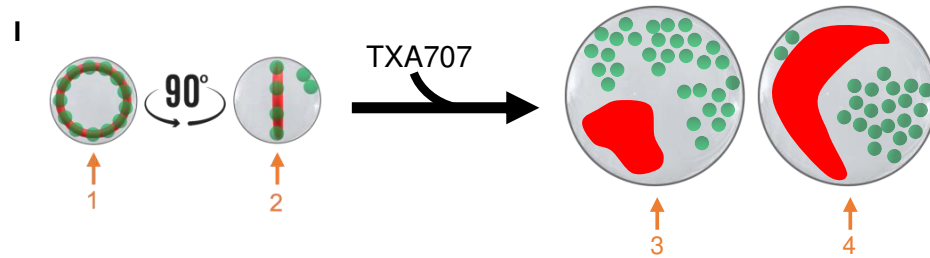
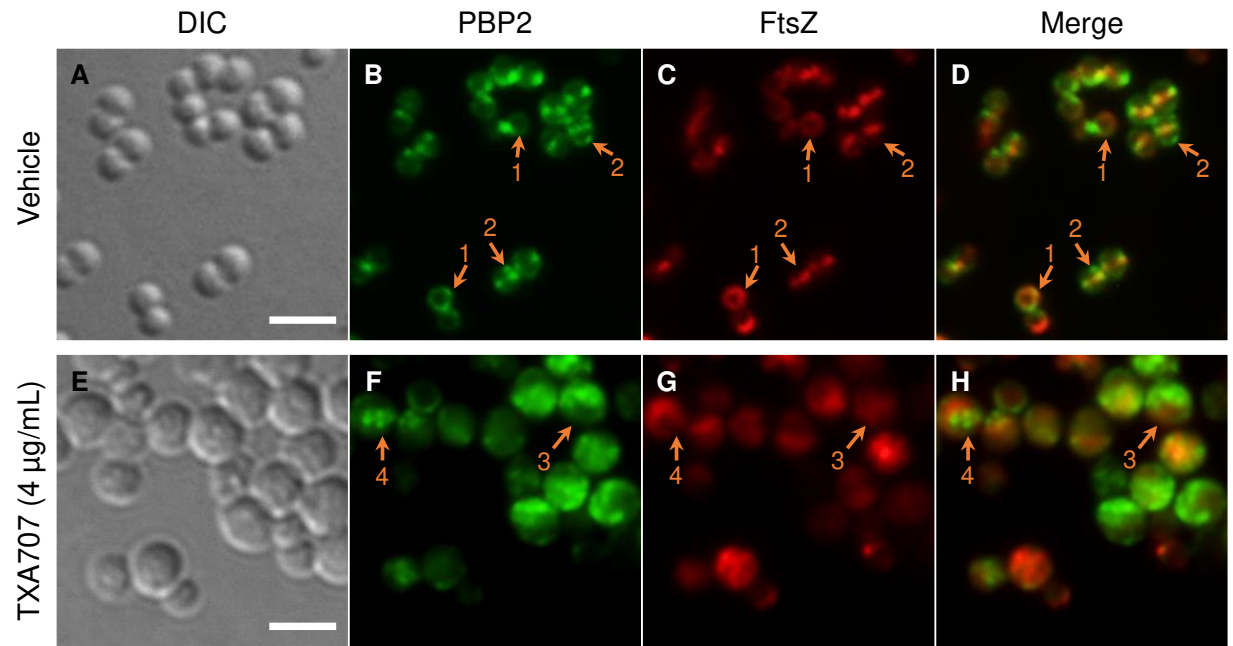


Figure 5

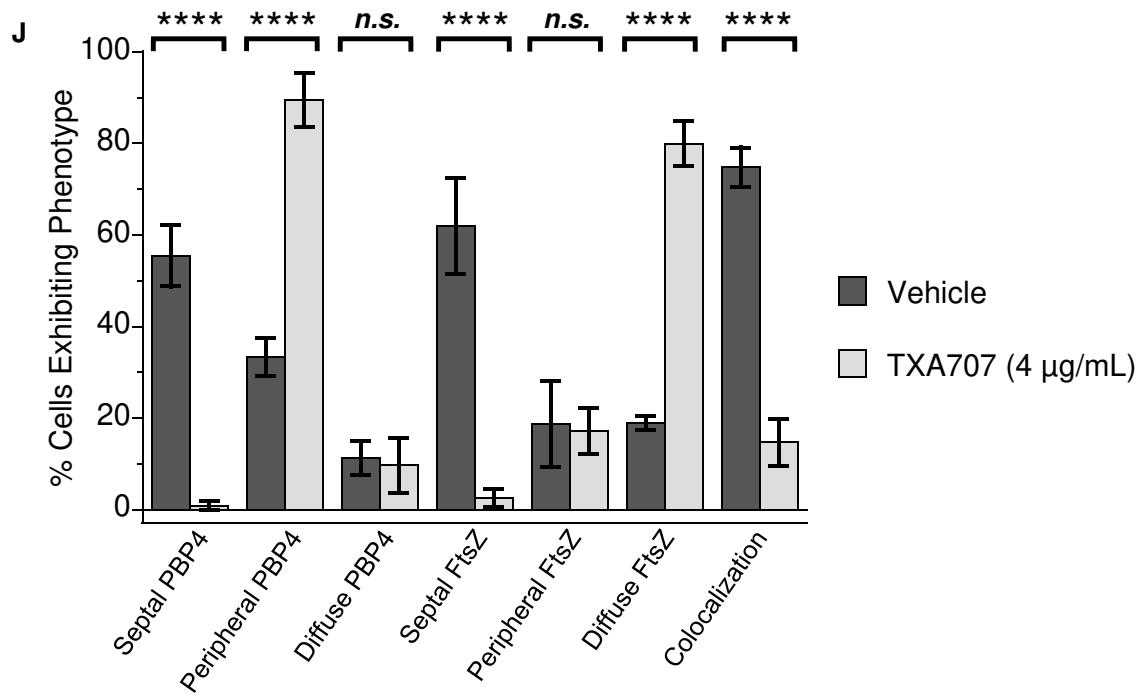
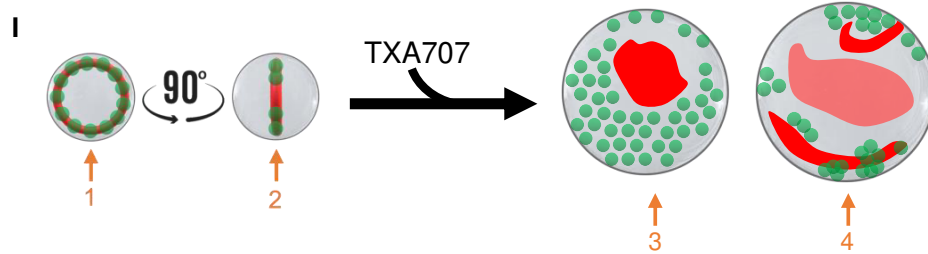
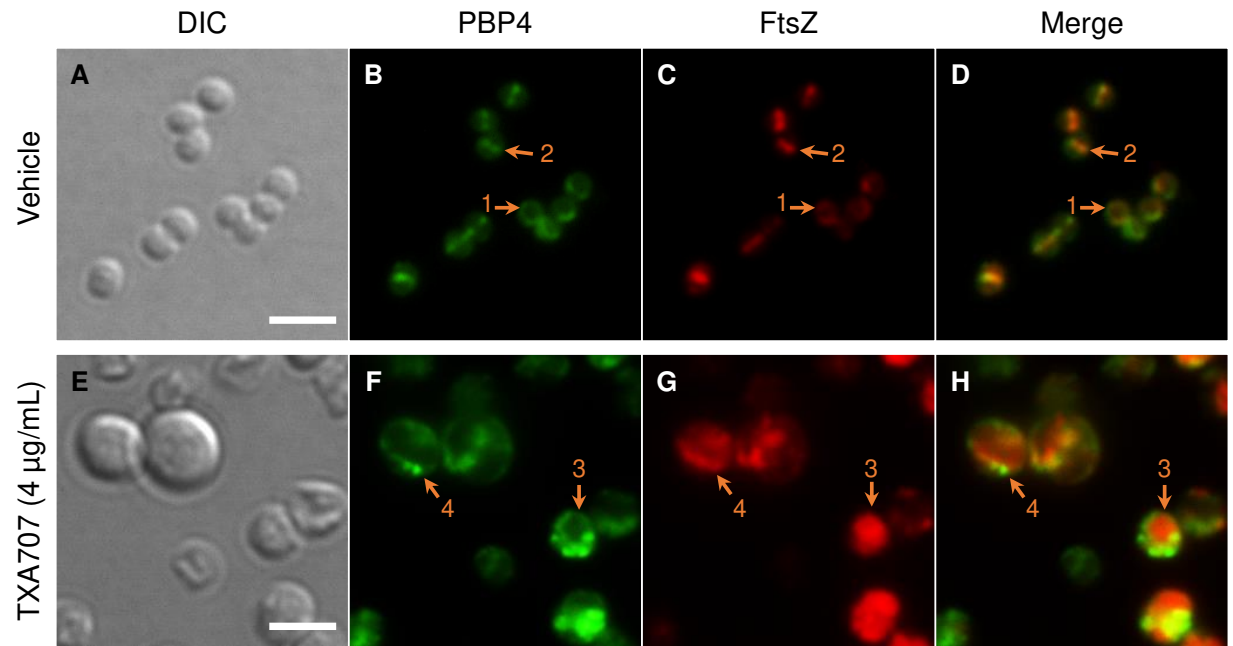


Figure 6

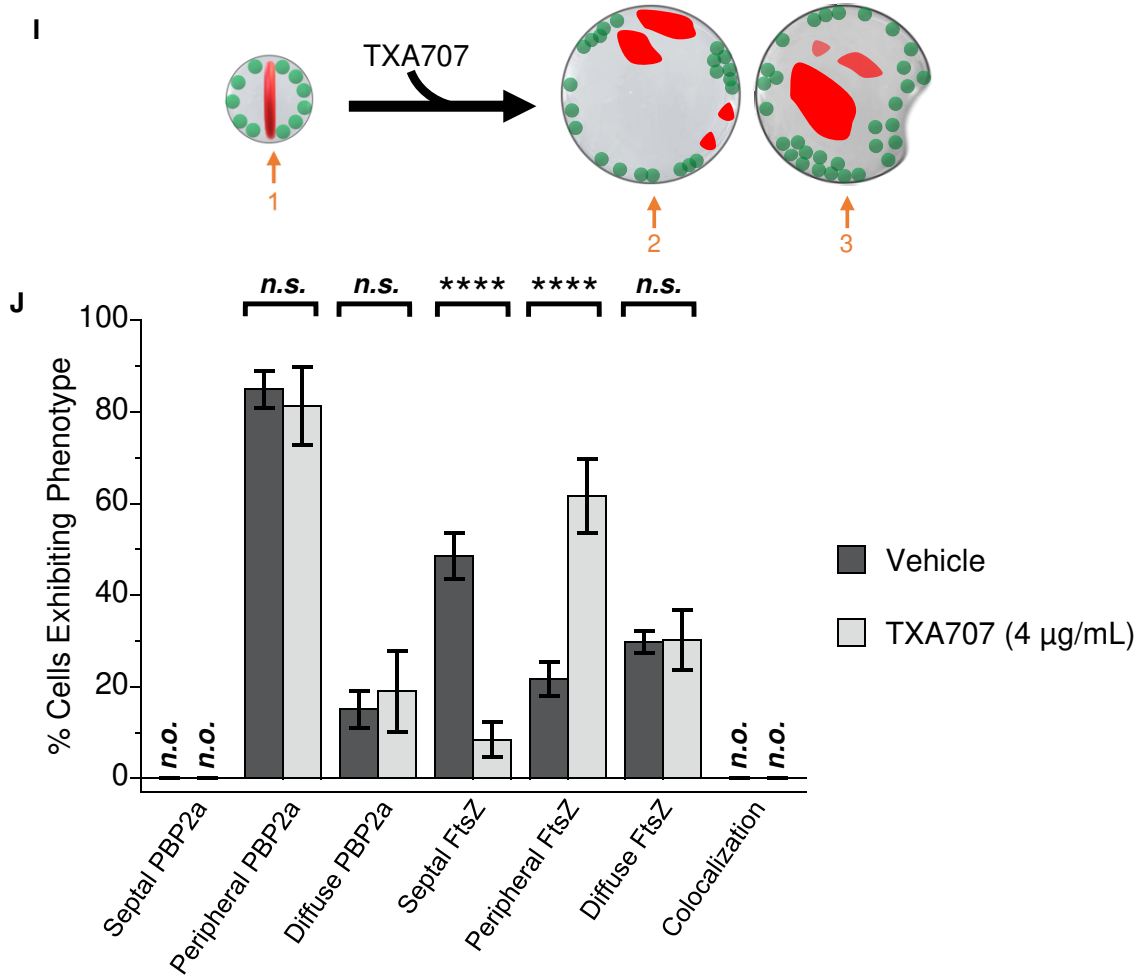
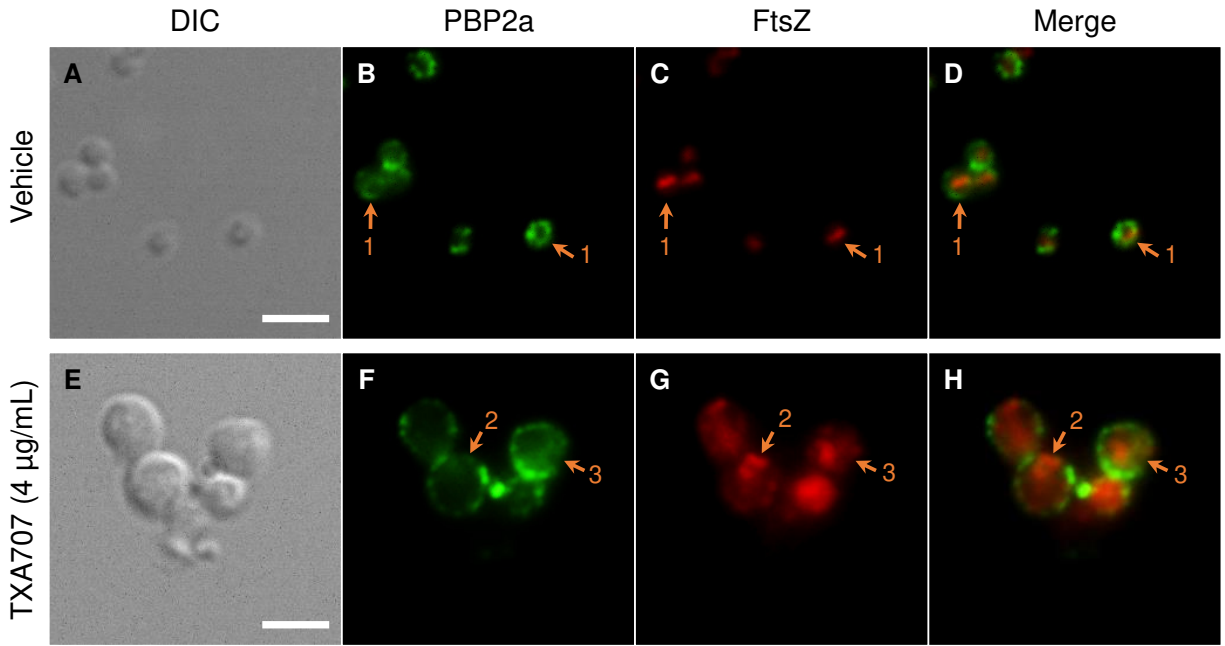


Figure 7

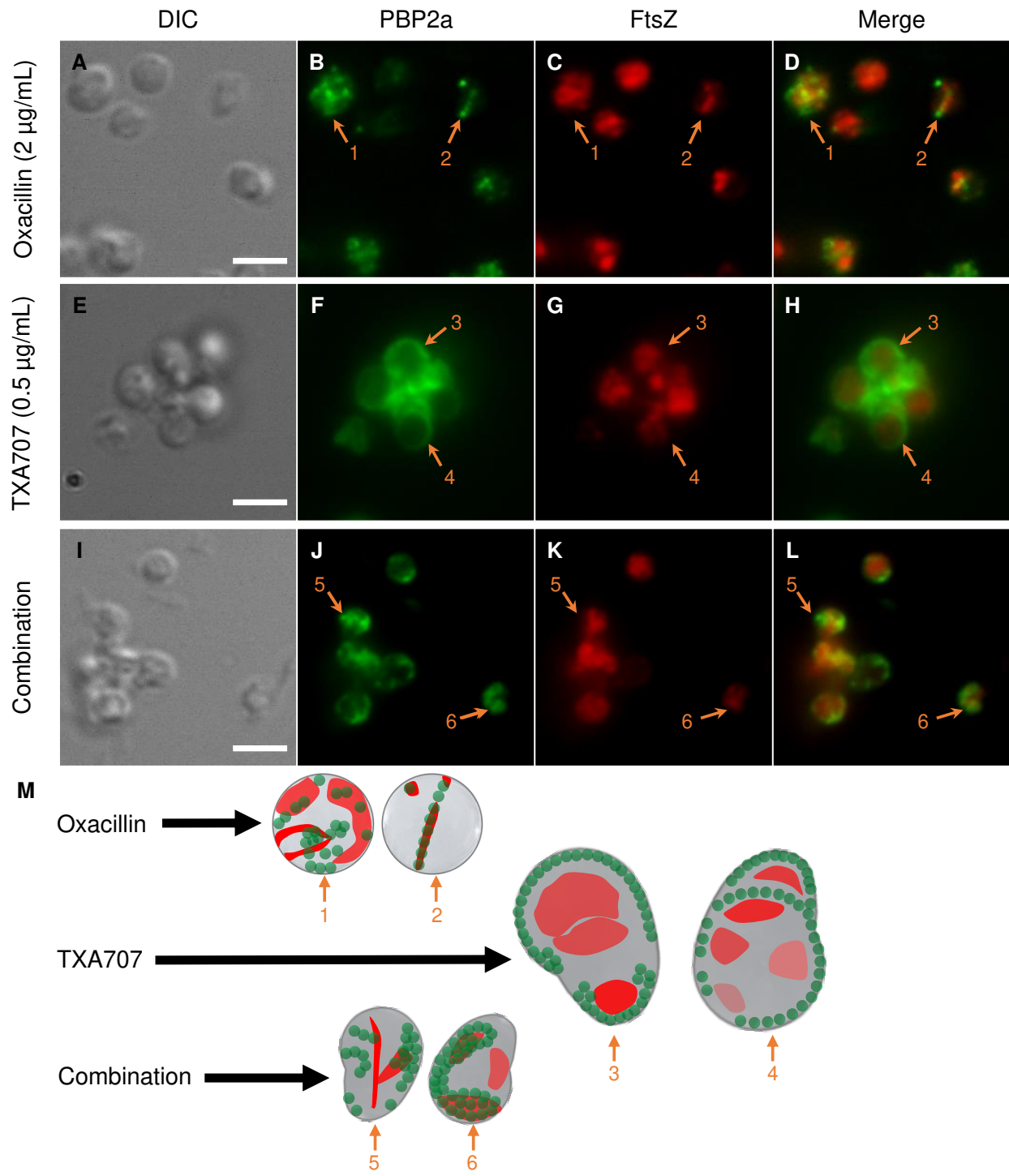


Figure 8

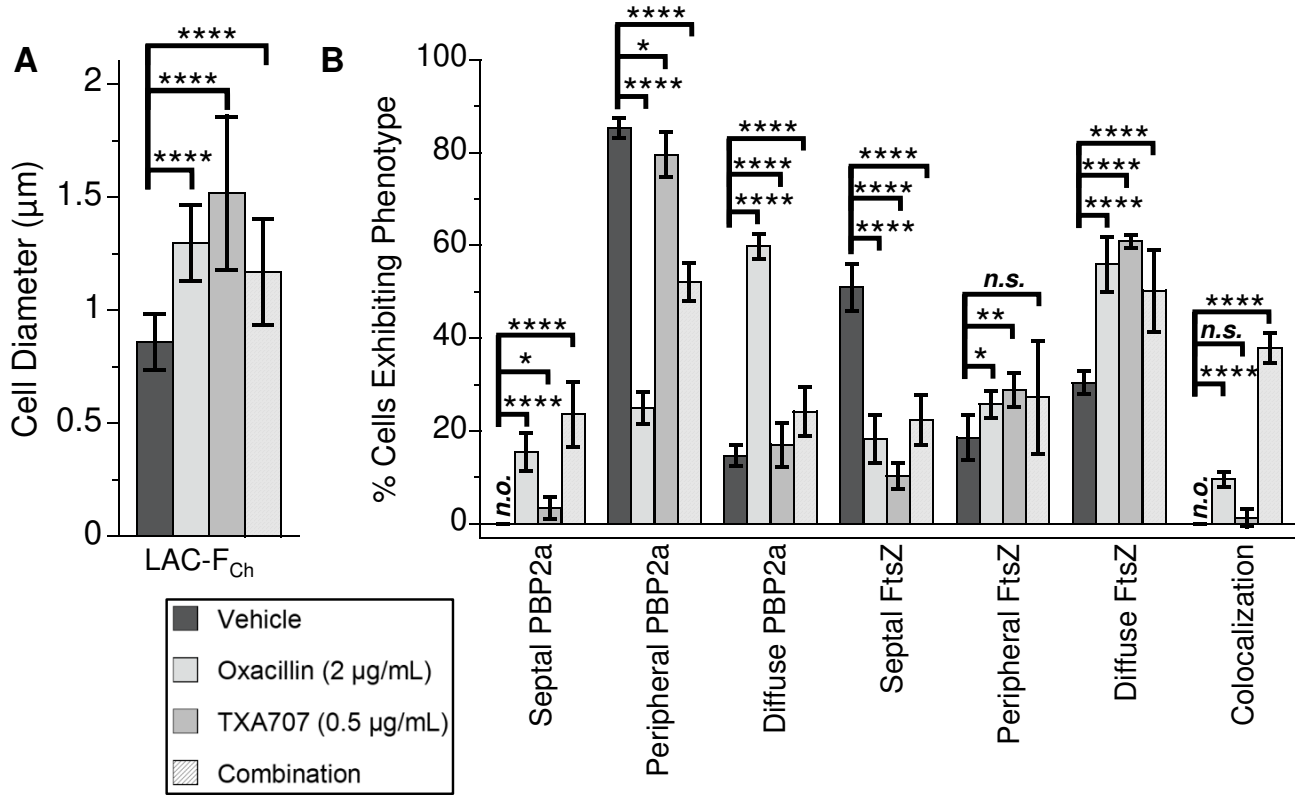


Figure 9

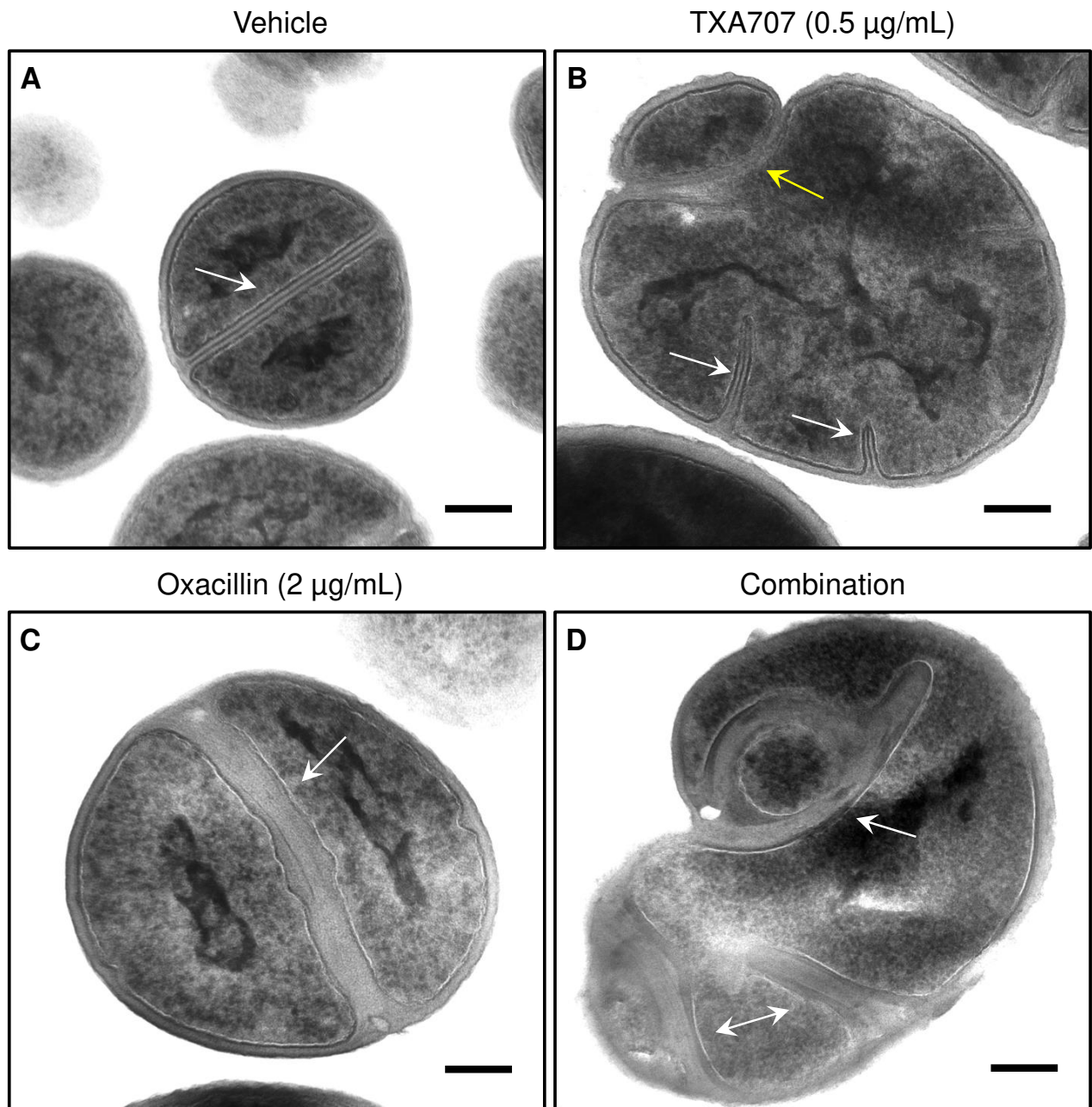


Figure 10

